

Episodic and Long-Term Sediment Transport Capacity in The Hudson River Estuary

David K. Ralston · W. Rockwell Geyer

Received: 1 September 2008 / Revised: 21 June 2009 / Accepted: 14 July 2009 / Published online: 6 August 2009
© Coastal and Estuarine Research Federation 2009

Abstract A tidally averaged model of estuarine dynamics is used to estimate sediment transport in the Hudson River estuary over the period 1918 to 2005. In long-term and seasonal means, along-channel gradients in sediment flux depend on the estuarine salinity gradient and along-channel depth profile. Lateral depth variation across the estuary affects the near-bottom baroclinic circulation and consequently the direction of net sediment flux, with generally up-estuary transport in the channel and down-estuary transport on the shoals. Sediment transport capacity in the lower estuary depends largely on river discharge, but is modified by the timing of discharge events with respect to the spring–neap cycle and subtidal fluctuations in sea level. Sediment transport capacity also depends on the duration of high-discharge events relative to the estuarine response time, a factor that varies seasonally with discharge and estuarine length. Sediment fluxes are calculated with the assumption that over long periods, the system approaches morphological equilibrium and sediment accumulation equals sea level rise. The inferred across- and along-channel distributions of sediment erodibility correspond with observations of bed properties. Equilibrium is assumed at long time scales, but at annual to decadal time scales the estuary can develop an excess or deficit of sediment relative to equilibrium. On average, sediment accumulates in the estuary during low- and high-discharge periods and is exported during moderate discharge. During high-discharge

periods, maximum export coincides with maximum sediment supply from the watershed, but the nearly cubic discharge dependence of fluvial sediment supply overwhelms the roughly linear increase in estuarine transport capacity. Consequently, sediment accumulates in the estuary during the highest flow conditions. Uncertainty remains in the model, particularly with sediment properties and boundary conditions, but the results clearly indicate variability in the sediment mass balance over long time scales due to discharge events.

Keywords Estuarine sediment transport · Episodic discharge events · Morphological equilibrium · Hudson River estuary

Introduction

Estuaries efficiently trap sediment and accumulate deposited material (Schubel and Hirschberg 1978). Rivers deliver sediment into the upper estuary and gravitational circulation transports marine sediment from the seabed and shoreline erosion into the lower estuary (Postma 1967; Meade 1969). Suspended sediment concentrations and the rate at which sediment accumulates in an estuary depend on the rate of sediment supply and on the hydrodynamic conditions, with feedbacks between hydrodynamics and sediment transport producing equilibrium morphologies. For example, if the water column deepens due to erosion or dredging, flow area increases, velocities decrease, and deposition increases until bed accretes to an equilibrium depth. Many estuaries are near morphodynamic equilibrium, where long-term sediment accumulation rates correspond to the rate of sea level rise (Meade 1969; Olsen et al. 1993). Disturbances such as dredging, infilling, or changes in watershed sediment supply can shift an estuary away from equilibrium and induce sedimentation or scour (Panuzio 1965; Bokuniewicz

D. K. Ralston · W. R. Geyer
Woods Hole Oceanographic Institution,
Woods Hole, MA 02543, USA

D. K. Ralston (✉)
Applied Ocean Physics and Engineering, MS #11,
Woods Hole Oceanographic Institution,
Woods Hole, MA 02543, USA
e-mail: dralston@whoi.edu

and Ellsworth 1986; Olsen et al. 1993; McHugh et al. 2004; Klingbeil and Sommerfield 2005).

The Hudson River estuary offers a well-documented example of estuarine sediment transport processes (Panuzio 1965; Woodruff et al. 2001; Geyer et al. 2001). The Hudson is a partially mixed estuary with the salinity intrusion ranging between 30 and 120 km upstream from the Battery, depending on river discharge and tidal forcing (Abood 1974; Ralston et al. 2008). The Mohawk and Upper Hudson Rivers converge 250 km upstream from the Battery and together supply between 0.2 and 1.0 million metric tons (MT) of sediment annually (Panuzio 1965; Olsen 1979; Ellsworth 1986; Woodruff 1999; Wall et al. 2008). The long-term accumulation rate in the estuary is consistent with the rate of sea level rise of 1–3 mm/year (Olsen et al. 1978; Hirschberg et al. 1996; Carbotte et al. 2004; McHugh et al. 2004; Klingbeil and Sommerfield 2005; Slagle et al. 2006), although short-term accumulation rates can be significantly greater (Sommerfield 2006).

Two distinct regions with persistently high suspended sediment concentrations have been identified as estuarine turbidity maxima (ETM). The lower ETM is located 12–20 km up-estuary from the Battery near the George Washington Bridge (Geyer et al. 2001; Traykovski et al. 2004), while the upper ETM is 55–60 km up-estuary in Upper Haverstraw Bay (Bokuniewicz and Arnold 1984). The ETMs feature high suspended sediment concentrations and localized accumulation rates that exceed the long-term mean. In the lower ETM, near-bottom concentrations can exceed 1,000 mg/L (Geyer et al. 2001; Traykovski et al. 2004) and short-term accumulation rates can be 10–30 cm/year (Olsen et al. 1978; Feng et al. 1998; Geyer et al. 2001; Woodruff et al. 2001). At tidal time scales net accumulation can be greater, with 1–4 cm of accumulation in a tidal period (Woodruff et al. 2001; Traykovski et al. 2004).

The 100-fold discrepancy between long- and short-term accumulation rates in the lower ETM presents an apparent contradiction. Most observations indicate that the local short-term sediment trapping is much greater than the volume required to maintain equilibrium with rising sea level. One hypothesis is that relatively infrequent large-magnitude storm events erode and export sediment to balance the sediment accretion during low to moderate river discharge. Stratigraphic evidence in the lower ETM indicates that decadal to centennial scale events scour material that is trapped at monthly to yearly time scales (Klingbeil and Sommerfield 2005). Geochronology of a resistant subsurface layer in the lower ETM dated a recent major erosion event to several years before 1954 (Klingbeil and Sommerfield 2005). Extreme events may also have the opposite effect of providing a large net input of sediment to estuaries if supply exceeds export. In Chesapeake Bay, just two major storms supplied half of the

total sediment input between 1900 and 1975 (Schubel and Hirschberg 1978).

The time scales of suspended sediment variability include tidal cycle resuspension, meteorological events of a few days, the fortnightly spring–neap cycle, seasonal river discharge, inter-annual droughts or wet periods, and decadal or longer recurrence intervals for extreme events. In the Hudson higher discharge occurs during the spring freshet ($\sim 2,000 \text{ m}^3 \text{ s}^{-1}$) and lower discharge during the late summer ($\sim 200 \text{ m}^3 \text{ s}^{-1}$). Recent observations also indicate a high-discharge period November through January that is less evident in the long-term record (Wall et al. 2008). Fluvial sediment load (Q_s) from upstream varies seasonally, typically depending on the discharge (Q_r) raised to a power between 1.5 and 2.5 (Nash 1994). In the Hudson, the power law ($Q_s \sim Q_r^n$) varies with discharge. At low to moderate discharge ($Q_r < 500 \text{ m}^3 \text{ s}^{-1}$), $n \sim 1.5$, while at higher discharge $n \sim 2.9$ (Woodruff 1999). Extreme meteorological events disproportionately affect the long-term sediment budget because of the non-linear dependence of sediment load on discharge. Sediment load measurements from any single year cannot represent processes with natural variability over much longer time scales (Woodruff 1999).

Observations in the lower ETM of the Hudson have documented both intra- and inter-annual variability in sediment transport. During spring freshets with moderate to high discharge, sediment flux is down-estuary and sediment deposits in New York Harbor (Woodruff et al. 2001). In the summer months after the freshet, sediment flux is up-estuary toward the ETM (Hirschberg et al. 1996; Feng et al. 1999; Woodruff et al. 2001). However, during relatively low-discharge freshets, sediment flux may be persistently up-estuary because baroclinic trapping remains strong (Geyer et al. 2001). For example, the 1998 spring freshet moved sediment into the Harbor, but during the weaker freshet in 1999 sediment flux in the lower ETM remained up-estuary (Geyer et al. 2001; Woodruff et al. 2001). During the moderate freshet of 2001, sediment flux in the lower ETM was down-estuary at maximum discharge and then turned up-estuary during lower discharge summer months (Traykovski et al. 2004).

The goal of this work is to quantify the effects of extreme discharge events on sediment transport and long-term sediment budgets in the Hudson, and more generally in partially mixed estuaries. We are interested in the discrepancy between the short- and long-term rates of sediment accumulation, and in understanding how the mismatch depends on the intermittency of discharge events. Changes in river discharge are expected to affect both the sediment transport capacity of the estuary and the supply of fluvial sediment, with consequences for the net accumulation or export of sediment. By simulating conditions using historical forcing, we can quantify the factors that affect transport such as event timing with respect to the tidal

forcing and event duration, as well as time scales of sediment retention in the system.

Model Description

To calculate sediment transport capacity over time scales ranging from days to decades, we use a tidally and cross-sectionally averaged model of the salinity and along-estuary velocity (MacCready 2007; Ralston et al. 2008). The model locally applies the quasi-steady Hansen and Rattray (1965) solution for residual shear and stratification to determine the subtidal baroclinic salt flux. The temporal evolution of the estuarine salinity distribution depends on the balance between the residual salt flux up-estuary and advection down-estuary due to the river discharge. The mean velocity is the river discharge modulated by subtidal water level fluctuations at the downstream boundary. At meteorological time scales (3–5 days), volume flux due to sea level fluctuations can increase the mean velocity by a factor of 2 or reverse the mean flow toward up-estuary (Bowen and Geyer 2003; Ralston et al. 2008). The model was calibrated and tested against salinity and velocity observations at multiple locations along the Hudson during 2004. Model inputs and the sediment transport calculations are described here, but the development, calibration, and application of the model are described elsewhere (Ralston et al. 2008).

Model Inputs

Model simulations ran from 1918 to 2005, producing subtidal salinity and velocity fields along the estuary. Inputs include bathymetry (depth $H(x)$ and cross-sectional area $A(x)$), tidal velocity amplitude $U_t(x,t)$, mean velocity $U_0(x,t)$, and salinity at the open boundary $S_{bc}(t)$. Channel depth and cross-sectional area were derived from data from the Hudson River Estuary Program of the New York State Department of Environmental Conservation, the National Oceanic and Atmospheric Administration (NOAA), and the US Geological Survey (USGS; Stedfast 1980). The model domain was from 0 to 180 km from the Battery with discretization of 1 km. To account for depth variation between channel and shoals, cross-sections are subdivided relative to the median cross-sectional depth and averaged laterally to get channel (H_1) and shoal (H_2) depths along the estuary. In a rectangular channel, $H_1=H_2$, but in a cross-section with broad, shallow shoals, $H_2 \ll H_1$.

Discharge data were collected from USGS stream flow gages (Fig. 1). From 1946 to present, discharge was determined from measurements at Green Island Dam (#01358000), about 250 km north of the Battery. For prior years, we combined discharge measurements in the tributaries that converge upstream of Green Island: the

Mohawk River at Cohoes (#01357500, from 1917) and the Upper Hudson River at Waterford (#01335754, from 1887). When measurements from all three stations were available, the sum of the tributary discharges agreed with the measurement at Green Island. The gage discharge was multiplied by a factor of 1.6 to account for tributaries downstream of Green Island based on comparisons between gage data and observations of mean flow in the lower estuary (Lerczak et al. 2006).

Mean velocity depends primarily on the river discharge, with $U_0 = Q_r/A$. However, subtidal water level fluctuations at the downstream boundary change the volume of the estuary and thus U_0 . Water level data (η_{bc}) during the observation period were taken from a NOAA tide gage at the Battery (#8518750; Fig. 1). Hourly water level data at the Battery was available as far back as 1958, so prior to that and during periods when the Battery station was out of service the tide gages at Sandy Hook (#8531680) and Atlantic City, NJ (#8534720) were used to determine the subtidal sea level variability. The Battery, Sandy Hook, and Atlantic City water level records were highly correlated at subtidal frequencies because of their proximity relative to the large-scale forcing that generates coastal set-up or set-down.

Tidal velocities determine vertical mixing rates and thus affect estuarine circulation and stratification. We use tidal current harmonic predictions to calculate U_t (Fig. 1). We incorporate spatial variability in U_t based on predicted current speed ratios at 24 stations along the Hudson referenced to The Narrows, New York Harbor, and interpolate between stations onto the model grid by conserving tidal volume flux. Current speeds are calculated using the T_TIDE software package (Pawlowicz et al. 2002) and harmonic constituents from the XTide software¹. Node factors and equilibrium arguments prior to 1970 are taken from the Institute of Ocean Sciences Tidal Package (Schureman 1959; Foreman 1978).

Without long-term observations of near-bottom salinity at the Battery or in New York Harbor, we base S_{bc} on correlations with Q_r and U_t . Salinity in the Harbor decreases with increased river discharge. A quasi-empirical relationship was developed in which we assumed that salinity gradient scales as $Q_r^{-1/3}$ (Abood 1974; Monismith et al. 2002; Ralston et al. 2008). The origin of the estuary with oceanic near-bottom salinity (S_0) is an unknown distance from the Battery. The salinity at the Battery varies as $S_{bc} = S_0(1 - c_1 Q_r^{1/3})$, where c_1 is a constant fit based on observations (Fig. 2a). The available bottom salinity data include tidally averaged observations in 2004 and instantaneous measurements at stations in the Harbor.

Generally S_{bc} decreased with river discharge, but the scatter about the best-fit relationship to Q_r was significant. The misfit depended in part on spring-neap variability in

¹ <http://www.flaterco.com/xtide/>

Fig. 1 Time series of forcing during model period (1918–2005): river discharge (Q_r), tidal velocity amplitude (U_t), and subtidal water level (at the Battery, η_{bc}). Periods of salinity observations (from USGS, WHOI, and NYCDEP) for model validation are indicated above the top panel

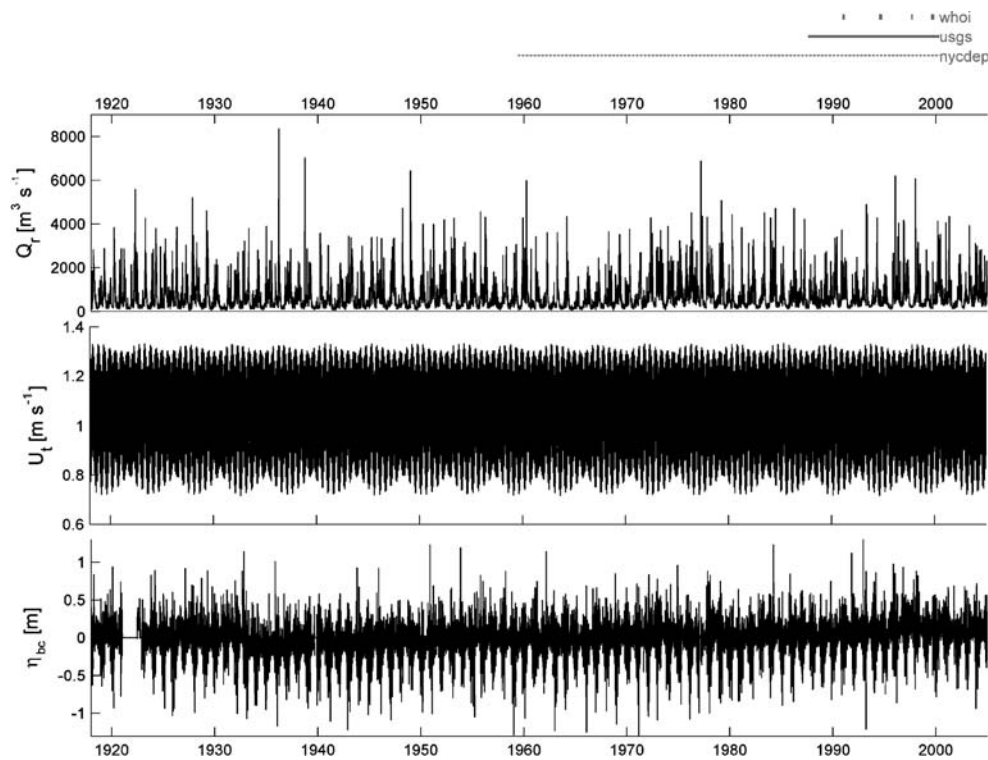
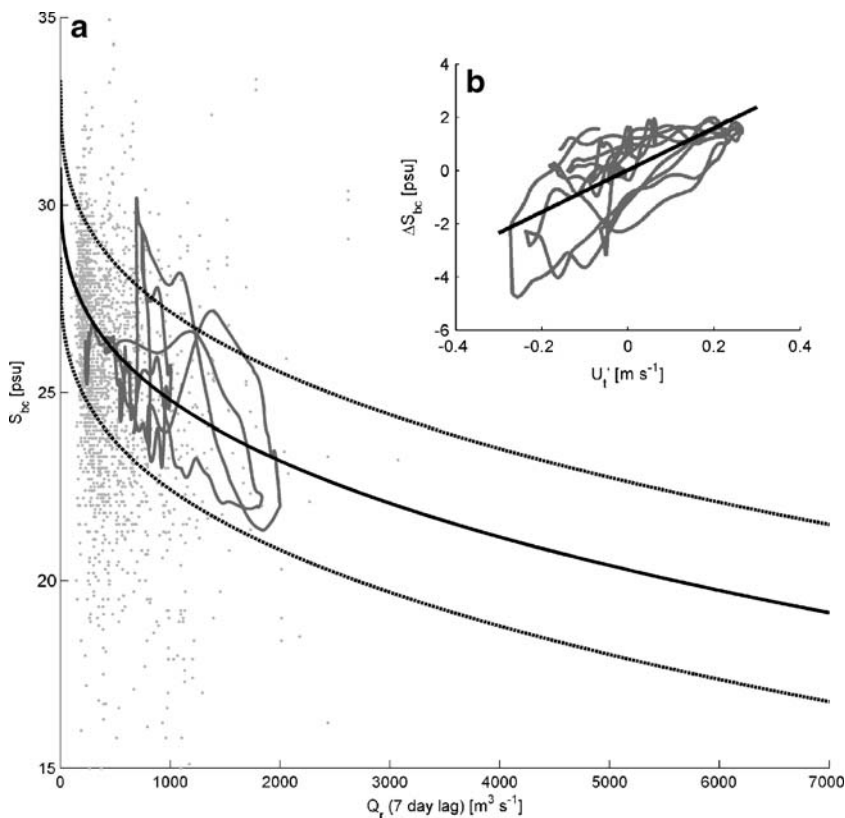


Fig. 2 Bottom salinity boundary condition at the Battery as function of Q_r (lagged 7 days) and U_t . **a** Observed bottom salinity at the Battery (subtidal time series in 2004, dark gray) and in New York Harbor (instantaneous measurements from 1968 to 2005, light gray) vs. Q_r . Solid line is $S_{bc} = S_0(1 - c_1 Q_r^{1/3})$, where $S_0=31$ and $c_1=0.020$. Dashed lines show $S_{bc} = S_0(1 - c_1 Q_r^{1/3}) - c_2 U_t'$ with $c_2=7.9$ and $U_t'=\pm 0.3 \text{ m s}^{-1}$, the range of tidal velocity variability. **b** Plot of salinity boundary condition misfit based on Q_r alone ($(S_{bc} - S_0(1 - c_1 Q_r^{1/3}))$) and tidal velocity variability ($U_t' = U_t - \bar{U}_t$). Slope of line is c_2 in Eq. 1



tidal mixing. During spring tides, mixing decreased stratification and near-bottom salinity for a given depth averaged salinity. During neaps, stronger stratification corresponded with higher near-bottom salinities. We accounted for variability in S_{bc} due to tidal mixing by fitting the difference (ΔS_{bc}) between observed salinities during 2004 and the prediction based on Q_r alone to U'_t , where $U'_t = U_t - \bar{U}_t$ and \bar{U}_t is the long-term average U_t (Fig. 2b). The salinity boundary condition was

$$S_{bc} = S_0 \left(1 - c_1 Q_r^{1/3} \right) - c_2 U'_t, \quad (1)$$

where c_2 is determined from the linear fit between ΔS_{bc} and ΔU_t . The parameters fit from the observations were $S_0 = 31$ psu, $c_1 = 0.020$, and $c_2 = 7.9$. S_{bc} calculated from Q_r and U_t produced simulations that better matched salinity observations in the estuary than using a constant S_0 .

Calibration and Validation

The model is calibrated by adjustment of two parameters that scale the vertical mixing of momentum and salinity. These mixing coefficients were optimized by comparison with salinity and velocity at multiple locations along the Hudson during the spring and summer of 2004 (Ralston et

al. 2008). The simulations presented here use the coefficients found for the 2004 period, but we validated the model by comparison with additional salinity observations (Fig. 3). The model skills (as defined in Ralston et al. 2008 and Warner et al. 2005) for the longer simulation period were similar to the detailed observations in 2004, and compared well with the skills reported for a three-dimensional hydrodynamic model of the Hudson (Warner et al. 2005). The model skill over the extended period for bottom salinity was 0.96 and for surface salinity was 0.97 (R^2 of 0.89 and 0.91, respectively).

To compare against observations over an even longer period we use surface and bottom measurements from the New York City Department of Environmental Protection (NYCDEP) monitoring of the lower Hudson. The NYCDEP has regularly visited seven stations from the Battery to 25 km up-estuary, primarily during summer months. The model corresponds with the observations, albeit with scatter likely due tidal cycle variability (Fig. 4). The model agrees more consistently with surface observations, but tends to over-predict bottom salinity. The bottom salinity discrepancy could be due to errors in the open boundary condition, or could be due to field sampling outside of the channel thalweg that would bias observed salinities low. Comparisons between instantaneous and tidally averaged quantities

Fig. 3 Time series of surface (dashed) and bottom (solid) tidally averaged salinity observations (black), with corresponding model results (gray). Locations range from 6 to 83 km and are indicated on the map. The source of observations (WHOI or USGS) are also indicated

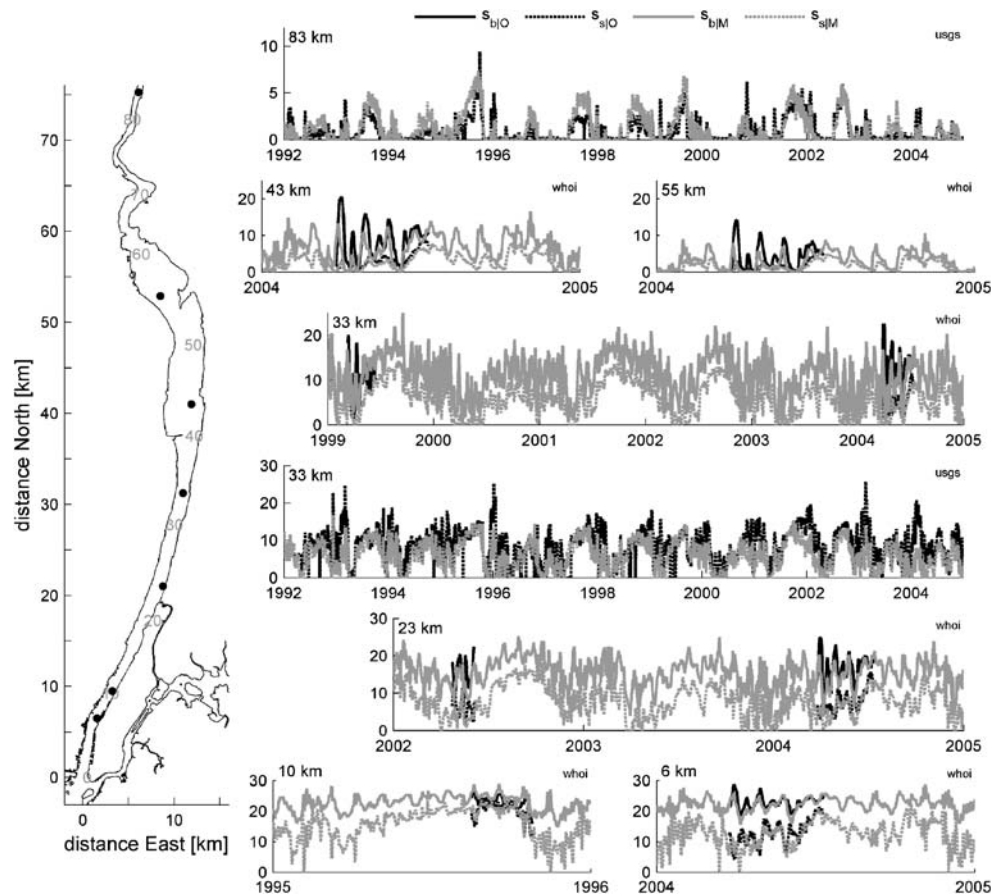
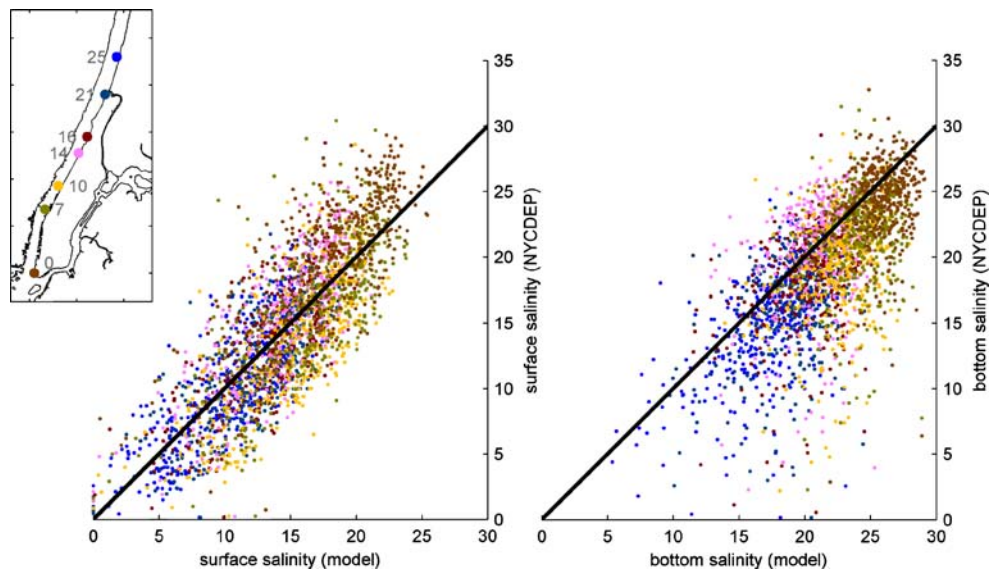


Fig. 4 Instantaneous surface and bottom salinity observations from NYCDEP (1968–2005) and corresponding tidally averaged model results. Colors indicate distance of sampling station from Battery (0 to 25 km), as shown in the map



are not ideal, but the historical observations generally support extension of the model to decadal time scales.

Near-Bottom Velocities

We use the prescribed (U_t) and calculated (U_0 , and estuarine velocity U_e) velocities to calculate the tidal maxima of near-bottom velocities during ebb and flood as functions of space and time. The estuarine velocity is the subtidal baroclinic circulation, and based on a frictional balance is calculated as $U_e = g\beta(\partial s/\partial x)H^3/(48K_m)$, where $\partial s/\partial x$ is the along-estuary salinity gradient, K_m is an effective eddy viscosity, and β is the coefficient of saline expansivity ($7.7 \times 10^{-4} \text{ psu}^{-1}$; Hansen and Rattray 1965). The estuarine circulation is up-estuary near the bed and down-estuary near the surface, and U_e is part of the model solution because it depends on $\partial s/\partial x$.

The vertical structures of the velocity components are used to define near-bottom velocities: U_t and U_0 have parabolic distributions, while U_e has a cubic form with flow upstream near the bed and downstream near the surface (Hansen and Rattray 1965; MacCready 2004). The near-bottom velocity is the sum of the three velocity components, and the relative contribution of each differs between flood and ebb. During floods, U_e enhances near-bottom flow and U_0 retards it, while during ebbs the roles reverse. The model calculates conditions in the channel thalweg, so we account for lateral variation in depth to determine near-bottom velocities on the shoals. On the shoals, the estuarine circulation is much weaker than in the thalweg, and potentially can be directed down-estuary. The contribution of U_e to the near-bottom velocity on the shoals is determined by projecting the thalweg cubic estuarine velocity profile laterally to the near-bottom elevation of the shoals. Details on the velocity calculation can be found in the Appendix.

To evaluate the near-bottom velocity parameterization, we compare the model results with ADCP measurements at nine locations in the lower Hudson estuary over 4 years (Fig. 5). The observations range from near the Battery to 44 km up-estuary, and include both channel and shoal stations. The data have been processed into maximum near-bottom flood and ebb velocities, and model velocities have been calculated according to Eqs. A1 and A2. The model velocities and the observations correspond well, especially considering the wide range of conditions sampled. The model skill for near-bottom flood velocities was 0.91 (R^2 of 0.71) and for ebb velocities was 0.95 (R^2 of 0.81). Note that these velocity observations were used to develop functions for parameters that depend on cross-sectional geometry to quantify the lateral distribution of velocity (see Appendix). Ideally, independent data from a different period or from a different estuary would be used to validate this model.

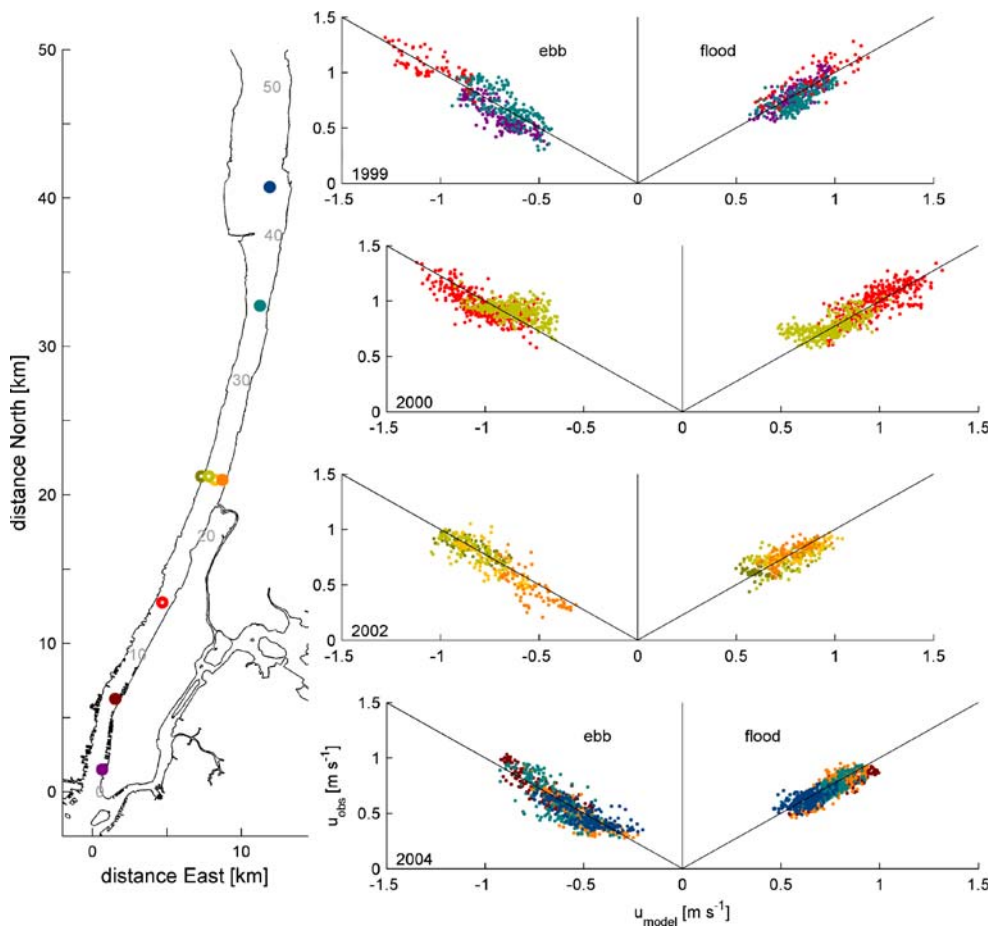
Sediment Transport and Transport Capacity

Sediment erosion rate depends on the excess bottom shear stress above a minimum threshold stress (Partheniades 1965). Based on this functional form and a correlation between excess shear stress and suspended sediment concentrations observed previously in the lower Hudson estuary (Traykovski et al. 2004), we calculate the tidal maximum sediment concentration (C_t) using a quadratic drag formulation for the excess bottom shear stress as

$$C_t = C_0 \frac{(U^2 - U_c^2)}{U_c^2} \quad U \geq U_c, \\ C_t = 0 \quad U < U_c \quad (2)$$

where U_c is a critical velocity for resuspension and C_0 is a reference concentration. Sediment flux depends on both sediment concentrations and velocities, and the net flux

Fig. 5 Comparison between modeled and observed near-bottom velocities. Panels on the right show data from different observation periods (1999 through 2004), and station location is indicated by color shown on map. Open markers on the map are stations on shoals; filled markers are stations in the thalweg



after a tidal cycle is the difference between up-estuary flux during the flood and down-estuary flux during the ebb. Sediment fluxes are sensitive to the erosion parameters U_c and C_0 that can vary spatially and temporally and are difficult to quantify in the field.

To address the uncertainty in the erosion parameters we take two approaches to estimate sediment transport. First we note that for reasonable values of U_c ($\sim 0.5 \text{ m s}^{-1}$), sediment flux is approximately proportional to U^3 . The net sediment transport capacity after a tidal cycle is

$$U_{\text{net}}^3 = U_{\text{flood}}^3 - U_{\text{ebb}}^3, \quad (3)$$

and U_{net}^3 is indicative of how sediment moves given an available supply of erodible material. When $U_{\text{net}}^3 < 0$, tidally averaged sediment transport is down-estuary or exporting, and $U_{\text{net}}^3 > 0$ represents net sediment flux up-estuary. Near-bottom velocities determine U_{net}^3 , incorporating both sediment resuspension proportional to bottom shear stress and net advection resulting from tidal asymmetry in the sense of the estuarine and river velocities. We set U_c proportional to the minimum local tidal velocity amplitude, and for U_{flood}^3 or $U_{\text{ebb}}^3 < U_c$, the sediment flux

during that phase of the tide is zero. The spatial and temporal patterns of U_{net}^3 are not sensitive to U_c over a range of values (including $U_c=0$), but U_c does affect the magnitude of U_{net}^3 .

The U_{net}^3 approach does not directly quantify sediment flux, as it is independent of the erodibility C_0 and input from upstream or downstream boundaries. In subsequent sections, we derive the spatial variability in sediment erodibility based on simplifying assumptions to directly calculate sediment fluxes. Initially (Sections **Sediment Transport Capacity** and **Extreme Events**) we focus on the sediment transport capacity (U_{net}^3) that depends on fewer assumptions about sediment properties. U_{net}^3 reflects local resuspension and net sediment transport capacity. The sediment flux calculations (Sections **Erodibility and Morphological Equilibrium**, **Comparison with Sediment Observations**, and **Long-term Sediment Flux**) incorporate the transport capacity, but also incorporate the fluvial sediment supply and heterogeneity in sediment properties. The 1D model does not track sediment fluxes at high-spatial and temporal resolution, so the sediment flux calculations are representative of broader scales rather than a specific location.

Results

Sediment Transport Capacity

The along-estuary distributions of channel and shoal depths directly affect the estuarine sediment transport capacity (Fig. 6a). Averaging over the simulation period produces the long-term mean of sediment transport capacity in the channel and on the shoals (Fig. 6b). Positive U_{net}^3 corresponds with sediment transport up-estuary, and in much of the lower Hudson, mean near-bottom sediment transport in the channel is up-estuary. In shallower regions, mean sediment transport is predominantly down-estuary. The lateral difference in mean U_{net}^3 is largely due to estuarine circulation. In the channel, U_e enhances near-bottom velocities during floods and retards flow during ebbs, creating net flux in the flood direction. On the shoals, the contribution of U_e is much weaker (or reversed), so U_0 produces ebb-dominant fluxes.

Both channel and shoals have significant along-estuary variability in mean transport capacity. In the channel, the greatest up-estuary transport occurs near the lower ETM (~14 to 24 km); farther upstream U_{net}^3 magnitude decreases.

Near the Battery (<8 km) where the cross-section has relatively uniform depth, mean transport over the entire width is up-estuary. Farther north in the Tappan Zee and Haverstraw Bay (~40 to 60 km) the estuary has broad shoals and a relatively narrow, shallow channel. Net transport on the shoals is down-estuary, and net transport in the channel is nearly zero. The along-estuary gradients in U_{net}^3 depend on U_e , but also include effects of along-estuary change in cross-sectional shape.

The long-term mean of U_{net}^3 masks variability at meteorological, seasonal, and inter-annual time scales. During low-discharge periods, U_{net}^3 can be relatively steady, such as during a severe drought when transport was up-estuary in the channel and down-estuary on the shoals (Fig. 6c). The U_{net}^3 distribution reflects variability in U_t and U_e (response due to changes in mixing) over the 7-day period, as Q_r and U_0 were relatively steady. When Q_r and U_0 (including the sea level set-up or set-down) change rapidly, U_{net}^3 can change rapidly. During a 7-day period around a high-discharge event, U_{net}^3 in the channel transitioned from up-estuary transport prior to the storm to down-estuary transport with the increase in U_0 (Fig. 6d). Sediment transport on the shoals also fluctuated during that

Fig. 6 Sediment transport capacity $U_{\text{net}}^3 = U_{\text{flood}}^3 - U_{\text{ebb}}^3$ as a function of distance along the estuary, with positive values for sediment transport up-estuary. **a** Hudson bathymetry with the depth of the thalweg (black) and of the channel and shoals (gray). **b** Mean U_{net}^3 over model period (1918–2005) for channel (dark) and shoals (light). **c** U_{net}^3 for channel and shoals during a 7-day period of low Q_r (August 19 to 25, 1964, $Q_{r,\text{mean}}=150 \text{ m}^3 \text{ s}^{-1}$, $Q_{r,\text{max}}=170 \text{ m}^3 \text{ s}^{-1}$). **d** U_{net}^3 for channel and shoals during 7 days with high Q_r (December 29, 1949 to January 4, 1949, $Q_{r,\text{mean}}=4,300 \text{ m}^3 \text{ s}^{-1}$, $Q_{r,\text{max}}=6,400 \text{ m}^3 \text{ s}^{-1}$)

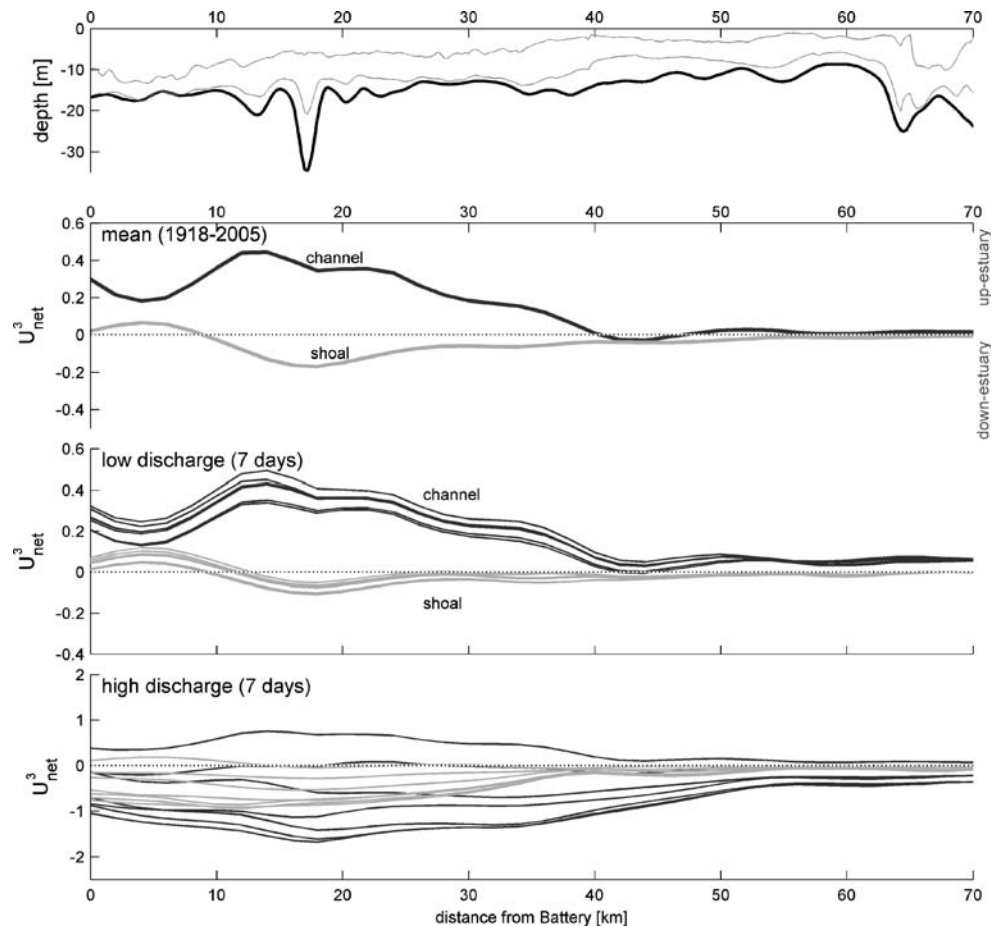
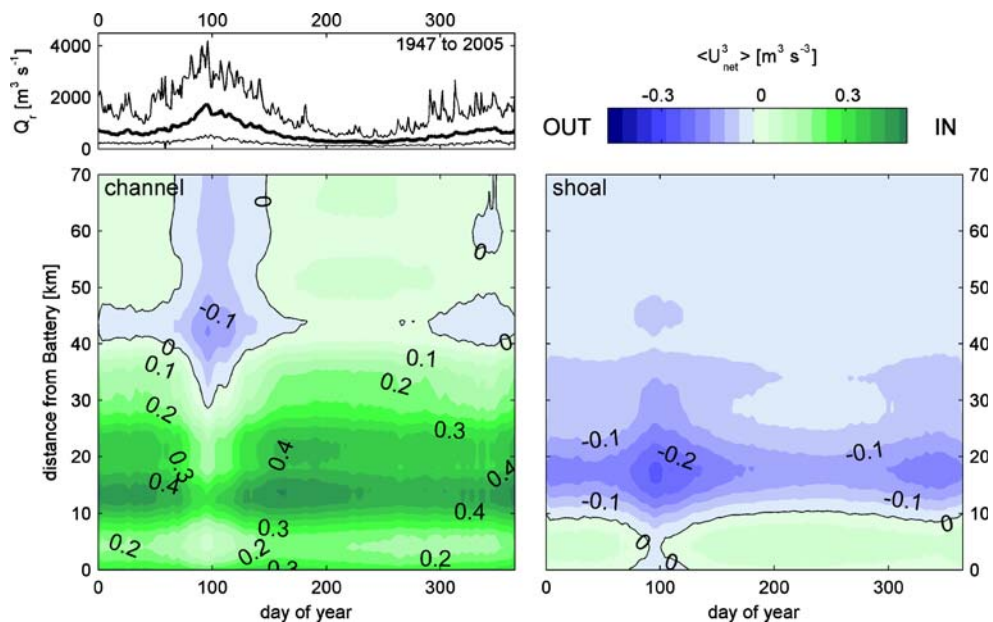


Fig. 7 Spatial and temporal maps of sediment transport capacity for the channel and shoals, plotting U_{net}^3 averaged over the period 1918–2005 as a function of distance along the estuary and day of the year. Upper panel shows seasonal discharge in the Hudson including mean, 5th and 95th percentile discharges (Green Island USGS station #01358000 from 1946 to 2005, multiplied by 1.6 to account for watershed inputs downstream of gage)



period, including a period of up-estuary transport when sea level set-up reversed the direction of U_0 .

The seasonal variability in U_{net}^3 depends largely on the annual cycle of river discharge (Fig. 7). During the spring freshet (day ~70 to 140), the salinity intrusion and region of up-estuary transport in the channel are confined to the lower estuary. The maximum sediment transport capacity on the shoals occurs during the freshet, when river velocities augment down-estuary transport. During lower discharge summer months, up-estuary transport in the channel expands northward into Haverstraw Bay. During the late fall and winter, the channel of the upper estuary shifts back toward down-estuary transport as Q_r increases.

Extreme Events

The seasonally averaged sediment transport capacity may not correspond with long-term transport if infrequent but large discharge events dominate the total flux. In the lower estuary ETM (16 km) and to the north of the ETM (34 km), U_{net}^3 exhibits temporal variability due to meteorological events (Fig. 8). U_{net}^3 at each station is approximately normally distributed around the long-term means, with channel transport strongly up-estuary in the ETM and decreasing in magnitude to the north. Transport on the shoals is largely down-estuary at both stations. However, extreme values of U_{net}^3 corresponding with the tails of the histograms can be opposite the long-term mean. The normal distribution of U_{net}^3 depends on the spring-neap variability in tidal amplitude, but extreme values of U_{net}^3 depend on the combination of Q_r , U_t , and η_{BC} .

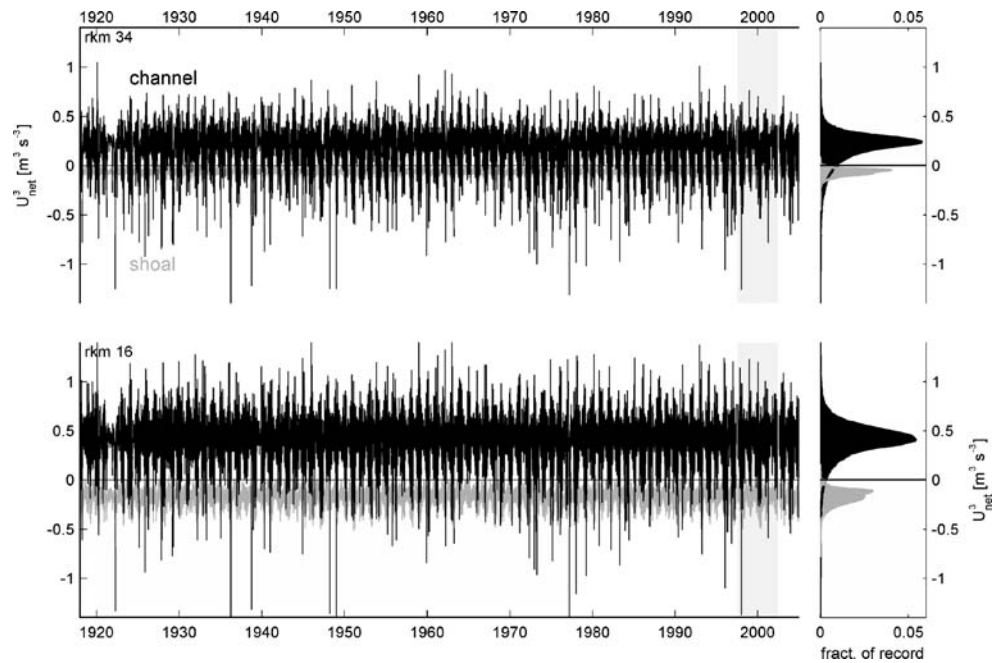
To highlight the variability at meteorological time scales, we focus on a period from 1998 to 2002 with sediment

transport observations in the lower Hudson (Geyer et al. 2001; Woodruff et al. 2001; Traykovski et al. 2004; Fig. 9). In January 1998, a high-discharge event ($Q_r \sim 6,100 \text{ m}^3 \text{ s}^{-1}$) generated strong down-estuary transport, both in the channel and on the shoals. In 1999, the freshet discharge was much weaker and net transport remained persistently up-estuary in the channel. The model results correspond with observations that down-estuary sediment flux during the 1998 freshet deposited material in the Harbor and the mobile sediment moved back up-estuary during lower discharge periods of 1998 and 1999 (Geyer et al. 2001; Woodruff et al. 2001). Another major discharge event occurred in April 2001 ($Q_r \sim 4,300 \text{ m}^3 \text{ s}^{-1}$), consistent with observations of down-estuary sediment flux in the lower ETM (Traykovski et al. 2004). After the freshet, flux in the channel shifted back up-estuary, also consistent with observations. Note that both 1998 and 2001 had relatively large flow events. The 1998 freshet ranked as the sixth largest event during the model period (1918–2005) and the 2001 freshet ranked 23rd.

In general, significant down-estuary sediment transport in the lower ETM results from high river discharge (Fig. 10). Focusing on the lower ETM (16 km), U_{net}^3 correlates with Q_r , particularly at large Q_r . In the channel, export occurs only at very high Q_r , as transport capacity remains up-estuary for Q_r less than about $3,000 \text{ m}^3 \text{ s}^{-1}$. Summing across the estuary, the correlation between U_{net}^3 and Q_r remains strong, but the transition from sediment import to export occurs at lower discharge ($Q_r \sim 1,500 \text{ m}^3 \text{ s}^{-1}$).

A few large discharge events dominated the down-estuary sediment flux. The highest river discharges from 1918 to 2005 were ranked as independent events if they occurred at least 7 days apart. During each independent

Fig. 8 Time series of sediment transport capacity U_{net}^3 with positive values for sediment transport up-estuary. Two locations are shown, in the lower ETM (16 km) and farther up-estuary (36 km), with results from the channel and shoals. Period shaded gray is shown in greater detail in Fig. 9



event, we identified the maximum sediment export based on U_{net}^3 , noting that in some cases the maximum export lagged the maximum Q_r by 1 or 2 days due to the adjustment of the salinity field. The 25 largest flow events and the U_{net}^3 during each event are highlighted, along with the relative magnitude of the tidal velocity during each event (Fig. 10). Transport capacity during the largest events

followed the general trend of greater export with larger Q_r , but with scatter due to the timing and duration of each event. If a discharge event occurred during spring tides, stronger tidal velocities enhanced vertical mixing and weakened the up-estuary transport by U_e . Spring tidal velocities during discharge events also enhanced the ebb-flood disparity in transport through terms such as $U_0 U_t^2$

Fig. 9 Time series of sediment transport capacity U_{net}^3 with positive values for sediment transport up-estuary. Two locations are shown, in the lower ETM (16 km) and farther up-estuary (36 km), with results from the channel and shoals. Period corresponds with observations discussed in Woodruff et al. (2001), Geyer et al. (2001), and Traykovski et al. (2004). Top panel shows discharge during the same period

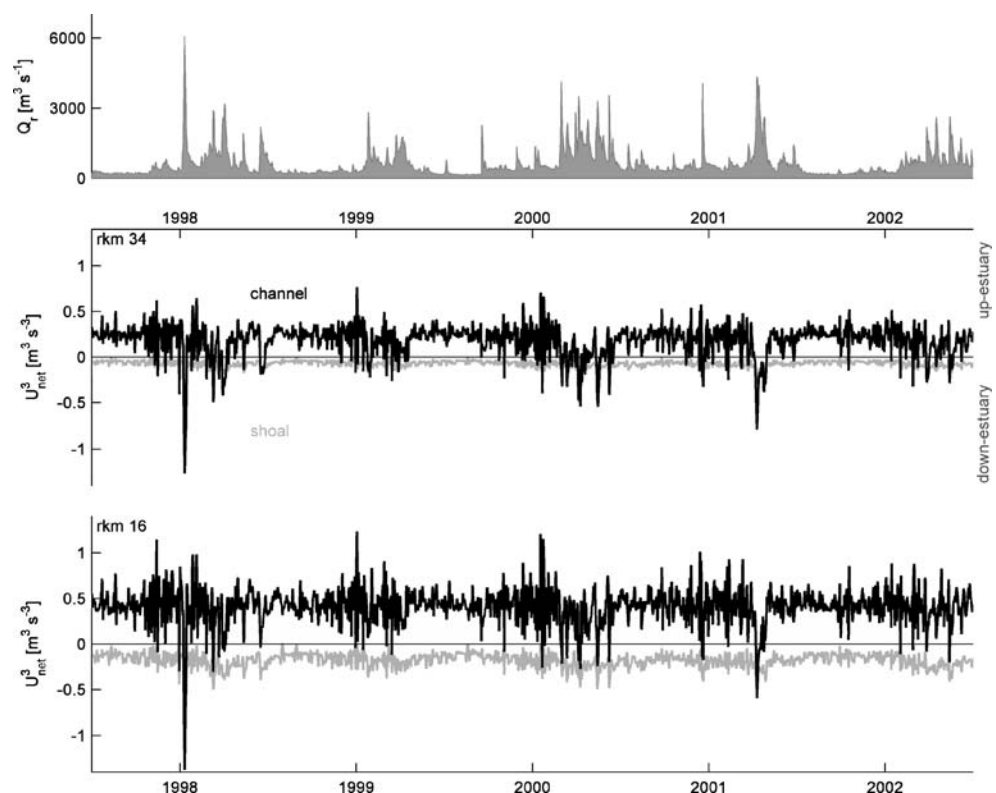
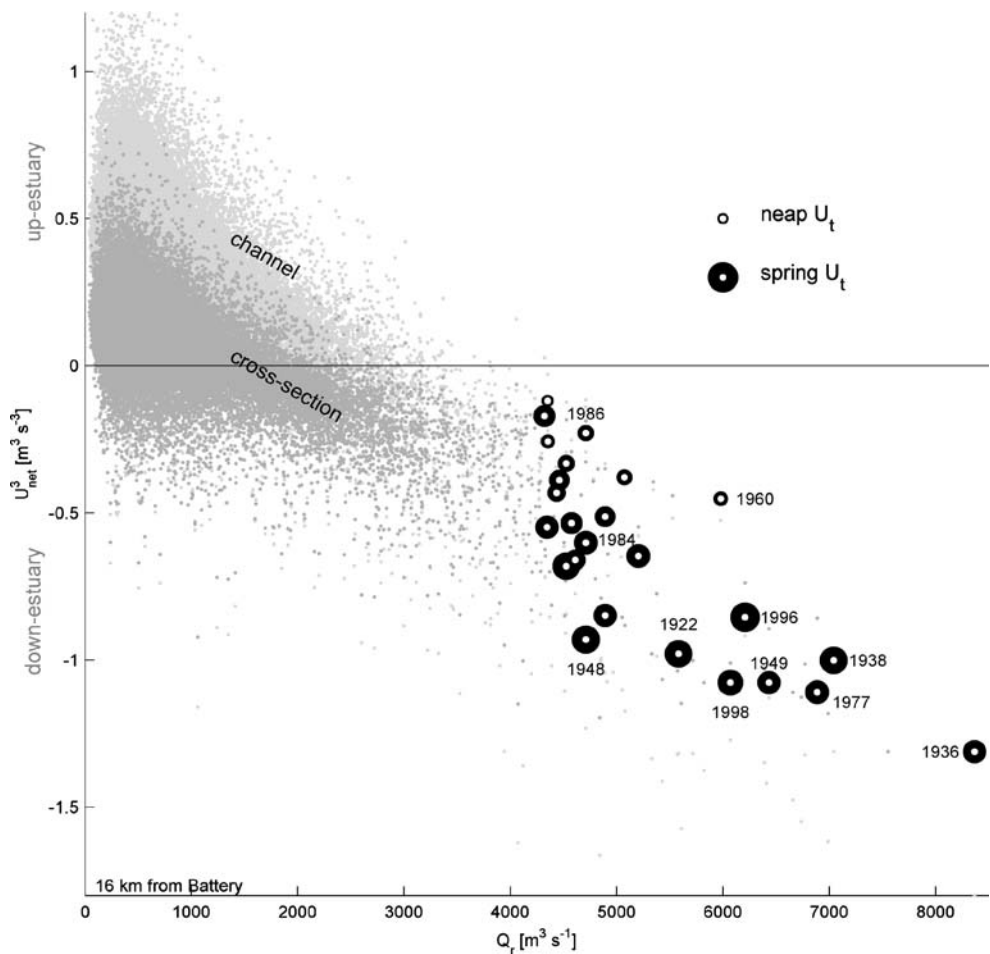


Fig. 10 Sediment transport capacity (U_{net}^3) in the lower ETM (16 km) vs. river discharge. Instantaneous values (every 0.5 day) are shown for the channel and the total cross-section. The 25 largest discharge events are identified with the maximum U_{net}^3 during each event. Additionally, the relative tidal velocity during the each event is indicated by the size of the marker. The dates of some of the largest events are indicated for reference. Large discharge events that occur during spring tides result in greater down-estuary transport than events during neap tides when estuarine circulation is stronger



from Eqs. 3 and A1. When a discharge event occurred during neap tides, mixing was weaker, estuarine circulation stronger, and transport in the lower estuary less likely to be down-estuary. Consequently, high-discharge events during spring tides had greater down-estuary transport capacity than similar magnitude flows during neap tides. For example, events in 1948, 1984, and 1986 (ranked #12, 13, and 14, respectively) all had discharges of about $4,700 \text{ m}^3 \text{ s}^{-1}$. The calculated U_{net}^3 during the three events varied widely despite the similar Q_r because of their timing with respect to the spring–neap cycle. The 1948 event during a spring tide had much stronger down-estuary transport than the 1986 event during a neap tide.

In addition to Q_r , U_0 depends on subtidal fluctuations in sea level due to coastal waves or storm surge. At low to moderate Q_r , variability in water level can alter the direction of sediment transport in the lower ETM (Fig. 11). Falling sea level transports volume out of the estuary and enhances sediment export, while rising sea level opposes river discharge and can generate net up-estuary transport. While the sea level forcing of mean velocity is important at lower Q_r , the largest sediment

export events remained linked to high Q_r . For high river discharge ($Q_r > 2,500 \text{ m}^3 \text{ s}^{-1}$ in Fig. 11), sea level fluctuations had a moderate effect on net transport, but the primary factors determining U_{net}^3 remained the magnitude of Q_r and timing with respect to U_t .

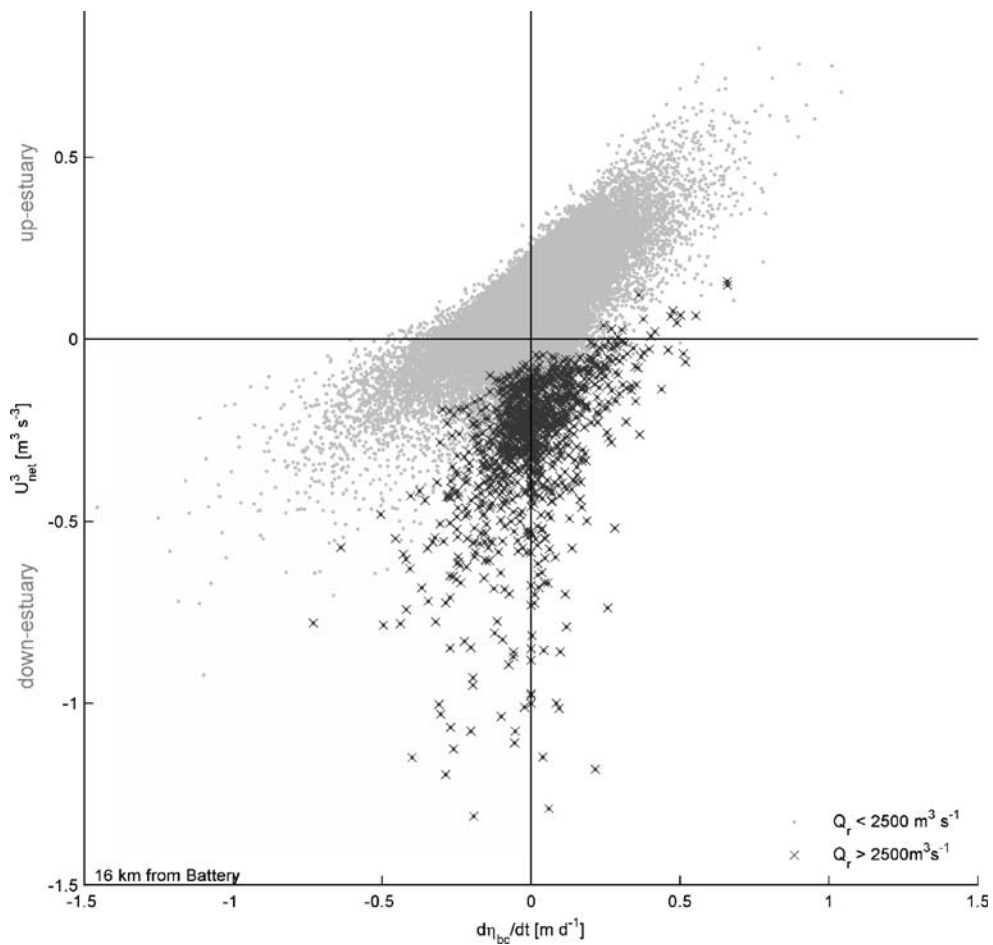
Erodibility and Morphological Equilibrium

U_{net}^3 is indicative of sediment transport capacity, but quantifying long-term sediment flux in the estuary requires assumptions about sediment properties, fluvial inputs, and the vertical distributions of $U(z)$ and $C(z)$. We start by assuming that the suspended sediment concentration decreases exponentially above the bed:

$$C(z) = C_t e^{-\frac{w_s}{K_m} z} \quad (4)$$

where w_s is the settling velocity, K_m is the eddy viscosity, and C_t is from Eq. 2. Settling velocities in estuaries vary spatially and temporally depending on sediment composition and flocculation, but here we use a representative value of $w_s = 0.5 \text{ mm s}^{-1}$ based on previous observations and

Fig. 11 Sediment transport capacity (U_{net}^3) in the lower ETM (16 km) vs. subtidal water level at the Battery ($\partial\eta_{\text{bc}}/\partial t$). Instantaneous values (every 0.5 day) of U_{net}^3 for the cross-section total are shown, distinguishing between periods with relatively high discharge ($Q_r > 2,500 \text{ m}^3 \text{ s}^{-1}$) and low to moderate discharge ($Q_r < 2,500 \text{ m}^3 \text{ s}^{-1}$). Volume flux due to falling subtidal water level can produce mean currents that can transport sediment out of the estuary, but the largest down-estuary transport occurs during high discharge events rather than due to fluctuations at the open boundary



modeling in the Hudson (Geyer et al. 1998; Traykovski et al. 2004). Eddy viscosities were taken from the model results, and typical values of 5 to 25 $\text{cm}^2 \text{ s}^{-1}$ produced vertical *e*-folding scales (K_m/w_s) from 1 to 5 m. We also tested a Rouse profile formulation for $C(z)$, but found that it yielded unreasonably high near-surface sediment concentrations compared with observations. The velocity profile was assumed to be parabolic, and the sediment flux was calculated as the depth integral of $U(z)C(z)$. Sediment flux remains proportional to U^3 as assumed previously, but the magnitude of the flux depends on w_s , C_0 , and U_c .

To determine C_t , we start with an initial assumption that erodibility C_0 is spatially uniform along the estuary and between channel and shoals. This simplification does not correspond with the heterogeneity observed in natural systems, but we use it as a null hypothesis to test whether lateral gradients in sediment properties are necessary for equilibrium transport. After demonstrating that spatially uniform erodibility does not satisfy the long-term sediment budget, we use the constraint of equilibrium transport to calculate the lateral heterogeneity in erodibility.

We initially assume that U_c scales with the minimum local tidal velocity amplitude ($U_c \sim 0.9 U_{\text{min}}$), and that $C_0 =$

0.4 kg m^{-3} everywhere. These values for U_c and C_0 correspond with suspended sediment observations from the Hudson lower ETM (Traykovski et al. 2004). Based on comparisons with observations of suspended sediment at Poughkeepsie (Wall et al. 2008), sediment erodibility is modified by a seasonal factor that varies with mean monthly temperature (Kirkby and Cox 1995). This approach supposes that winter storms erode sediment from unvegetated hillslopes and that the excess sediment input to the estuary deposits as a relatively unconsolidated, erodible bed. During summer months, sediment supply decreases and without resupply of new material, the bed becomes more consolidated, fine particles are winnowed away, and bed sediment is more resistant to resuspension. To reflect this we multiply C_0 by a seasonal scaling factor $s_f = 1 - (T - \bar{T})/\Delta T$, where T is the monthly mean temperature (at Albany), \bar{T} is the annual average, and ΔT is the annual range. Comparisons of this formulation with observations are shown in Section Comparison with Sediment Observations.

The sediment loading from the watershed was empirically based on daily discharge and sediment load (Q_s , tons day $^{-1}$) observations from the Mohawk River (at Cohoes)

and the Upper Hudson River (at Waterford). The sediment loads (Q_s) were fit to the form

$$Q_s = Q_{s0} \left(\frac{Q_r}{Q_{r0}} \right)^\alpha, \quad (5)$$

where Q_{r0} represents a transition between low and high-discharge conditions (Woodruff 1999). The sediment loading parameters for each river are given in Table 1. The total sediment loading is the sum of the Mohawk and Upper Hudson rating curve fluxes plus an additional 30% for sediment input by tributaries downstream of Green Island (Wall et al. 2008). Over the model period (1918–2005), the mean fluvial sediment load was 0.37 MT year⁻¹ at Green Island Dam and 0.48 MT year⁻¹ including downstream tributaries. The sediment loadings calculated from the rating curves were consistent to within 10% of observations: 0.72 MT during 1959–1960 (Panuzio 1965), 1.0 MT during 1976–1977 (Olsen 1979), and an annual average of 0.74 MT between 2002 and 2006 (Wall et al. 2008). The long-term average from the rating curve is significantly less than measurements during relatively high-discharge years of 1959–1960 and 1976–1977. Measurements at Poughkeepsie from 2002 to 2006 ranged annually between 0.68 and 0.83 MT, with an estimated 20% to 40% of the sediment input from tributaries downstream of Green Island (Wall et al. 2008).

Over long time scales, we assume that estuarine morphology approaches equilibrium such that the accumulation rates correspond with sea level rise (Meade 1969; McHugh et al. 2004; Klingbeil and Sommerfield 2005; Nitsche et al. 2007). Summed over the estuary, the accumulation required to keep pace with sea level rise of 2 mm year⁻¹ accounts for about 0.2 MT year⁻¹, roughly half of the long-term average input. To maintain morphological equilibrium, the estuary then must export the fluvial supply in excess of equilibrium accumulation. This equilibrium assumption constrains the long-term average sediment fluxes in the system so that we can solve for the implied distribution of erosion properties.

At each grid cell along the estuary, we calculate the erodibility (C_0) in the channel and on the shoal that yields the net sediment flux consistent with equilibrium morphology over the simulation period. Under our initial assumption that erodibility is laterally uniform, up-estuary flux in the channel of the lower estuary is greater than the down-estuary flux on the shoals (Fig. 12a). Consequently, the long-term sediment export would be insufficient to remove the fluvial input and sediment would accumulate in the lower estuary. For the system to maintain morphological equilibrium, bed sediment in the channel of the lower estuary must be more resistant to erosion than on the shoals. We solve for the necessary distribution of erodibility (C_0) such that at every position along the estuary the long-term mean sediment transport equals the difference between the fluvial sediment input and the bed accumulation corresponding to sea level rise. To constrain the calculation, we hold the erosion threshold U_c constant and solve at each location for the C_0 that meets the net flux constraint. Alternatively, C_0 and U_c could co-vary. If both C_0 and U_c were part of the solution the resulting bed sediment parameters would be quantitatively different but would produce qualitatively similar trends in erodibility along- and across-estuary.

To maintain long-term morphological equilibrium, bed sediment in the channel of the lower estuary must be more resistant to erosion than the adjacent shoals, or C_0 decreased in the channel and increased on the shoals (Fig. 12b). Farther north (40 to 50 km), the estuary widens and shallows, and a lateral gradient in sediment properties is not necessary because up-estuary transport in the channel is much weaker. Instead, both channel and shoal sediment must be more resistant to erosion than initially hypothesized to match the long-term sediment flux. Moving farther up-estuary (>50 km) the estuary becomes wider and shallower, and lateral variation in erodibility is required to maintain equilibrium long-term transport.

Comparison with Sediment Observations

To evaluate the sediment transport calculations, we compare the model results with suspended and bed sediment observations. Suspended sediment concentrations in the model depend on calculated near-bottom velocities, the sediment concentration formulation (Eq. 2), and the erodibility C_0 calculated from the long-term equilibrium assumption. Each of these steps introduces potential errors or erroneous assumptions can skew the results.

For comparison we use near-bottom sediment measurements in the lower estuary from observations in 1999 (Geyer et al. 2001) and 2000 to 2001 (Traykovski et al. 2004), including sites both in the channel and on the shoals (Fig. 13). We also evaluate the seasonal scaling factor for C_0 using a longer time series of suspended sediment at Poughkeepsie (124 km) (Wall et al. 2008). At Poughkeepsie, C_0 is a best fit to the observations rather than an independent result of the model simulation because the

Table 1 Parameters for fluvial sediment loading (Eq. 5; Woodruff 1999)

	Mohawk River		Upper Hudson River	
Q_{r0} [m ³ s ⁻¹]	500		400	
	$Q_r < Q_{r0}$	$Q_r > Q_{r0}$	$Q_r < Q_{r0}$	$Q_r > Q_{r0}$
α	1.35	2.87	1.43	2.87
Q_{s0} [tons day ⁻¹]	990	1,600	300	370

sediment calculations did not extend into the freshwater river. At locations in the estuary, C_0 is independently calculated from the equilibrium transport constraint (Fig. 12b) and the resulting sediment concentrations are compared with observations.

The model sediment concentrations are within a factor of 2 of the observed values, and at some stations the correspondence is much better. Spring–neap tidal variability in sediment concentration was observed at most sites, and the timing and the amplitude of the variability are reproduced in the model. The seasonal modulation of erodibility provides a better fit to the observations at Poughkeepsie (skill=0.85, $R^2=0.56$) than a constant C_0 (skill=0.50, $R^2=0.08$). Skill scores for suspended sediment in the estuary ranged between 0.84 ($R^2=0.67$) at 14 km and 0.35 ($R^2=0.08$) in the channel at 35 km.

The skills are significantly lower than for salinity or velocity, reflecting the uncertainty in the parameterization of the bottom boundary condition. We must emphasize that this modeling approach is not suited for detailed comparisons at high spatial or temporal resolution. The model is tidally averaged and the discretization is coarse both along- and across-estuary. Bed sediment properties are likely heterogeneous and unsteady at scales that are not captured in the model, but that affect observed conditions. Rather than highly resolved simulations of suspended sediment, the strength of this approach is to integrate over estuarine spatial scales and decadal time scales to capture lower frequency variability in sediment flux and accumulation.

A more integrative evaluation of the results is to compare the bed sediment properties derived from the model with bed sediment observations. A benthic mapping project² over the tidal extent of the Hudson River combined multi-beam bathymetry, side-scan sonar, sub-bottom profiling, and sediment cores to classify bottom sediment types and erosional or depositional regions (Nitsche et al. 2007). Erosional areas were defined as regions with high side-scan backscatter indicative of winnowing, scour, or armoring, higher sediment density, and larger grain sizes (Nitsche et al. 2004). Depositional regions had low side-scan backscatter, lower density sediment layers, and finer grain sizes. To directly compare the model results with the observed bed properties, we projected the map of sediment classifications (categories defined in Table 2 of Nitsche et al. 2007) on to the channel and shoal sections used here.

The fractional areas of the channel and shoal regions that were labeled depositional are plotted against distance from the Battery (Fig. 12c). Depositional regions correspond with bed sediment that was less consolidated and finer grained, and presumably more easily resuspended. Erosion-

al regions had bottom sediment that was more consolidated, coarser grained, and likely required greater energy to resuspend. In the lower estuary (<35 km), the channel was predominantly erosional and the shoals were depositional, consistent with lower C_0 in the channel where scour and armoring lend resistance to erosion and higher C_0 on the shoals where less consolidated sediments were more prone to resuspension. At the deep constriction near the George Washington Bridge (18 km) the shoals were locally more erosional, in agreement with the model decrease in C_0 . Up-estuary in the Tappan Zee (35 to 50 km), channel and shoals both were relatively erosional, consistent with decreased C_0 in this region. Up-estuary of 50 km in Haverstraw Bay, the model suggests the shoals are more depositional while the observations say the opposite. Here the estuary is significantly wider than in the lower estuary (<40 km), and wind waves may be important for resuspension and lateral redistribution of sediment, and may affect bottom properties on the shoals. Such wind effects are not incorporated in this model. Overall, the comparison between model and observed bed properties supports the hypothesis that lateral gradients in bed sediment properties are required to balance sediment flux, particularly in the lower estuary.

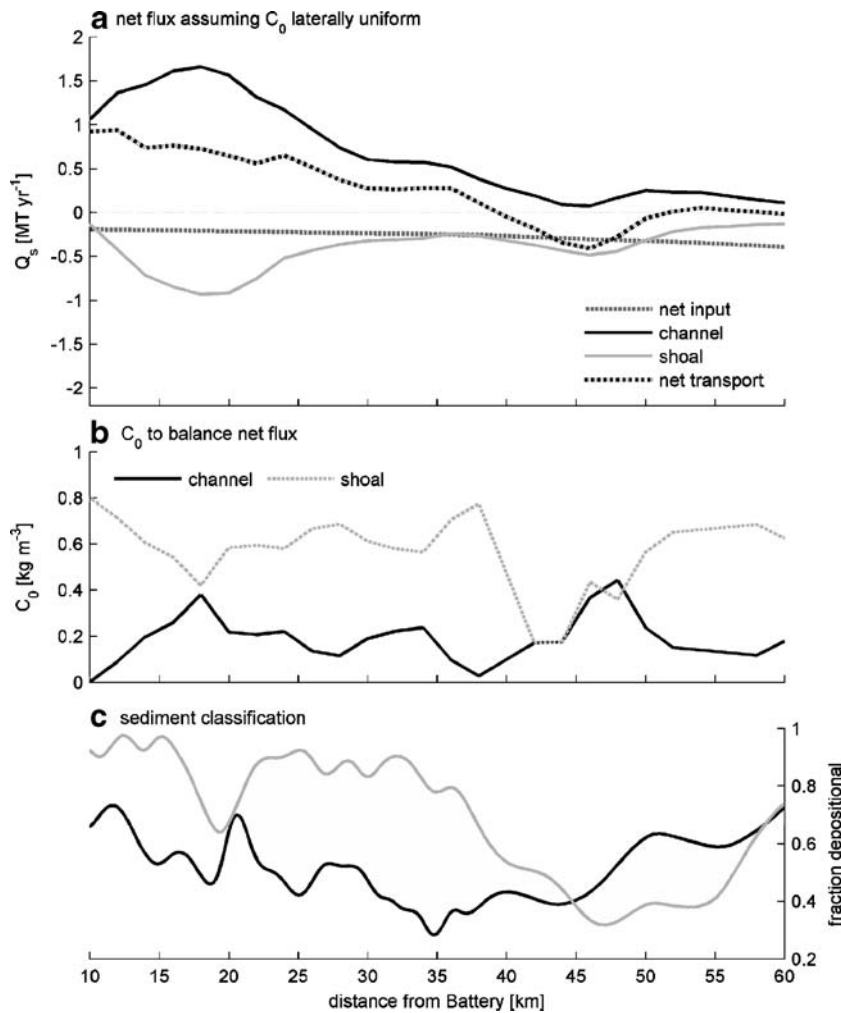
Long-term Sediment Flux

Based on the sediment rating curves and inferred distribution of C_0 , we calculated sediment fluxes as a function of time and distance along the estuary. Fluvial sediment input depended strongly on river discharge and was highly unsteady. Over annual to decadal intervals, the estuary had an excess or deficit of sediment relative to long-term equilibrium (Fig. 14). Annually, the freshet delivered sediment and subsequent moderate discharge periods provided net export from the system. This was consistent with radionuclide observations that indicated sediment residence times on the shoals of the lower ETM of 0.5–1 year (Feng et al. 1998). However, a sequence of particularly dry or wet years could produce more substantial accumulation or removal of sediment. For example, the 1960s were a period of severe drought, and millions of tons of sediment accumulated in the estuary. Average discharge increased in the 1970s, and estuarine transport removed sediment from the system.

The mass excess or deficit is indicative of the pool of the potentially mobile bed sediment. We converted the cumulative mass at each point along the estuary to an equivalent change in bottom depth by assuming laterally uniform deposition or erosion (Fig. 14). The maximum depth of accumulation or erosion was about 0.5 m, with accumulation greatest in the ETMs following the largest storm events and the drought of the 1960s. In reality, accumulation and

² <http://cugir.mannlib.cornell.edu/bucketinfo.jsp?id=7885>

Fig. 12 **a** Net sediment flux based on initial assumption of spatially uniform C_0 . **b** Reference concentration (C_0) distribution that satisfies long-term morphological equilibrium (net input rate equal to net transport). **c** Fraction of bed sediment in channel and shoal regions classified as depositional (Nitsche et al. 2007)



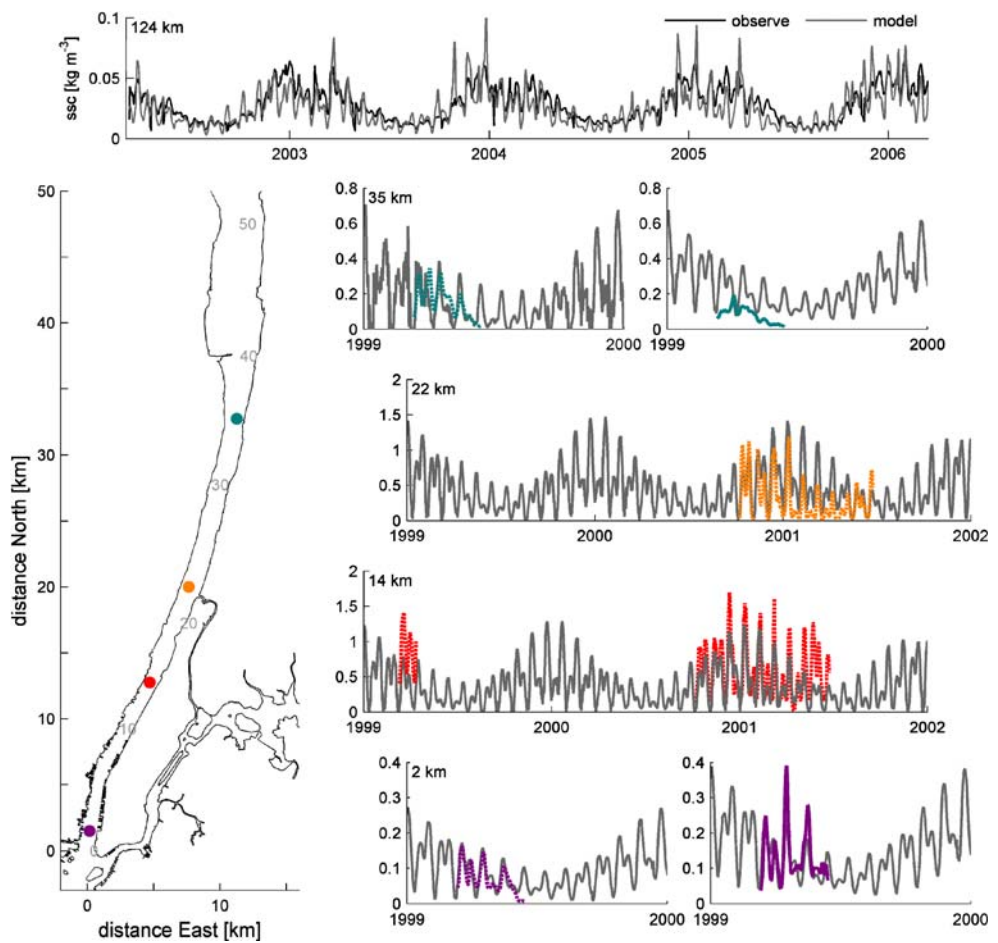
erosion may be localized on the shoals rather than laterally uniform across the estuary (Woodruff et al. 2001). Similarly, observations in the Delaware Estuary have shown that inter-annual storage of sediment in depositional regions can exceed the annual sediment input from the river (Cook et al. 2007).

Estuarine sediment transport capacity increases approximately linearly with discharge (Fig. 10), but fluvial sediment supply increases nearly cubically (Eq. 5). The net sediment flux depends on both factors (Fig. 15). During low discharge periods ($Q_r < \sim 400 \text{ m}^3 \text{ s}^{-1}$), estuarine circulation traps sediment in the estuary, with the greatest accumulation in the ETM regions. At moderate discharge ($Q_r \sim 400$ to $2,000 \text{ m}^3 \text{ s}^{-1}$), sediment flux is on average seaward as the estuarine transport capacity increases sediment export, especially on the shoals. During very high-discharge events ($Q_r > \sim 2,000 \text{ m}^3 \text{ s}^{-1}$), sediment input from the river is much greater than the estuarine transport capacity and excess sediment is stored in the system until it can be exported at more moderate Q_r . Note the discharge

dependence is only one factor, and that the substantial spread in net flux for a given Q_r demonstrates the importance of tidal amplitude and sea level fluctuations.

The sediment flux dependence on Q_r may appear to be at odds with the previous calculations of sediment transport capacity. According to U_{net}^3 , the greatest down-estuary transport occurs during the highest discharge events. In the sediment flux calculations, the estuary actually gains sediment during the highest discharge events, and net export only occurs at moderate Q_r . The discrepancy reflects the difference between the transport and the net convergence or divergence of sediment. The flux calculations include the fluvial sediment supply that is far more sensitive to Q_r than the estuarine sediment transport capacity. While estuarine transport is strongly down-estuary during high-discharge events, the increased transport is not sufficient to keep up with the increased supply of sediment from the watershed. The excess sediment must be stored in the estuary temporarily until it is exported during periods of moderate Q_r .

Fig. 13 Suspended sediment observations and model results. Data from 1999 are from near-bed optical backscatter sensors and data from 2000–2001 are from acoustic backscatter profiles. Dashed lines indicate observations on the shoals and solid lines are in the channel. Top panel is from USGS observations at Poughkeepsie (124 km) based on acoustical backscatter profiles



Discussion

Tidal Forcing

Extreme discharge events dominate sediment export in the channel of the lower estuary, but the relative impact of a given discharge depends on the coincident tidal velocities and the sea level forcing. Consequently, estimates of the probability of a given magnitude of transport must consider not only statistics of the basin hydrology, but also variability in tidal forcing and subtidal sea level (which may be correlated with Q_r). Tidal velocities in particular have a major effect on the potential U_{net}^3 . Significant down-estuary transport in the channel of the lower ETM requires simultaneously high discharge and strong tides. Leaving aside monthly to annual modulation of spring tidal amplitude, a discharge event has about a 20% probability of occurring within 1 day of maximum spring tides, and if the high discharge extends over 3 days then the odds increase to about 40%.

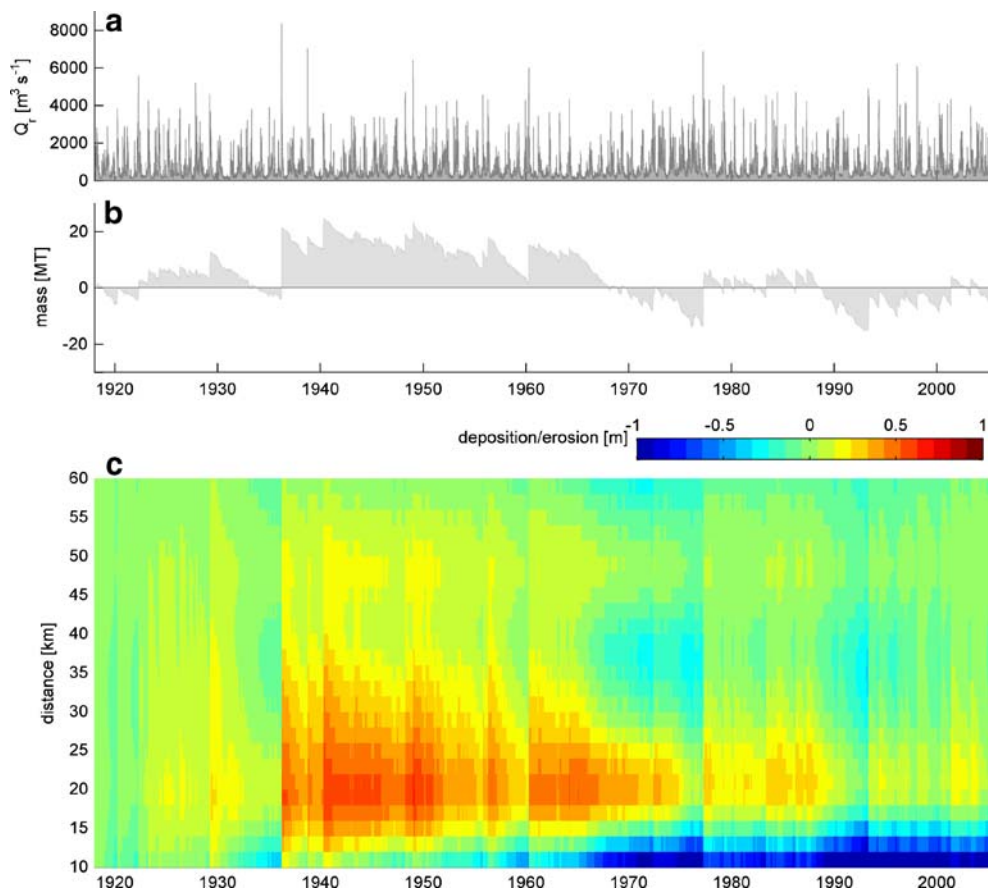
Large tidal velocities increase resuspension by eroding more deeply into bed sediment. Tidal amplitude also alters vertical mixing and estuarine circulation, affecting whether

suspended material moves downstream or remains in the estuary. Seismic reflection profiles and sediment geochronology indicated that a major erosion event occurred in the lower Hudson estuary several years prior to 1954 (Klingbeil and Sommerfield 2005). In the model results, two high-discharge events that coincided with spring tides occurred less than a year apart in March 1948 and January 1949 (Q_r ranked 12 and 4, respectively). With little time for sediment accretion between events, the second event may have eroded more deeply than if it had been isolated, producing an erosion-resistant layer still evident in the sub-bottom of the lower ETM.

Estuarine Response Time

In addition to the tidal forcing, sediment transport depends on the duration of discharge events relative to the estuarine response time. Estuaries adjust to changes in forcing over periods depending on the length of the estuary (L_x) and the freshwater velocity (Q_r/A) (Kranenburg 1986; MacCready 2007). Observations in the Hudson (Lerczak et al. 2008) and results from a 3D hydrodynamic model (Hetland and Geyer 2004) indicate that estuarine response times scale as

Fig. 14 Cumulative sediment mass. **a** Discharge. **b** Cumulative sediment mass in the estuary relative to long-term equilibrium with sea level rise. **c** Spatial distribution of accumulation or erosion relative to long-term equilibrium



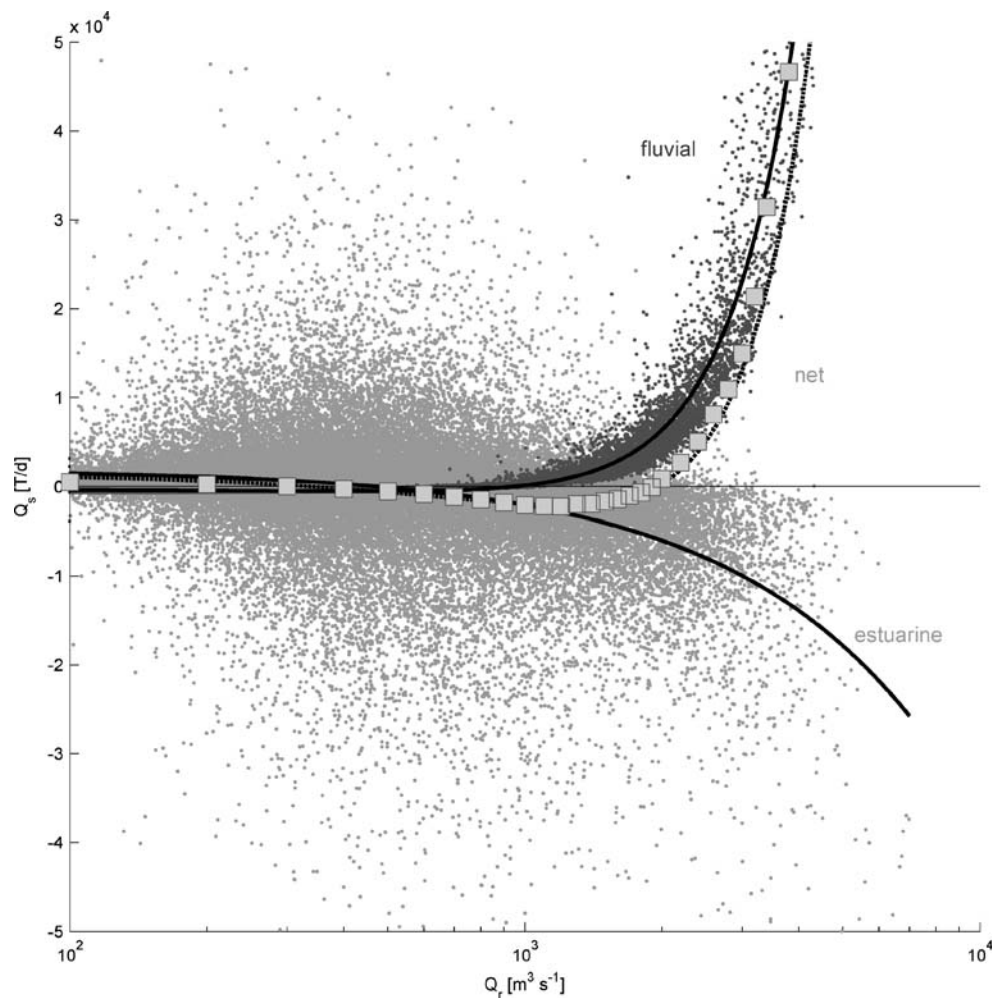
$T_{\text{response}} \sim L_x A / Q_r$. If a discharge event is shorter than the estuarine response time, then the salinity intrusion remains longer than its equilibrium and down-estuary sediment transport is reduced.

Spring freshets in the Hudson typically occur in March or April due to rain and snow melt with broad peaks of a week or longer. However, intense winter rain events can generate high discharges over just a few days. For example, winter storms in 1949, 1996, and 1998 had similar discharges ($\sim 6,000 \text{ m}^3 \text{ s}^{-1}$), and all occurred during spring tides (Fig. 10). Equilibrium scaling would predict similar salinity distributions and sediment transport for the three events, but the transport during the 1996 event was less than the other two cases despite stronger tides. The durations of the 1949 and 1998 events were approximately equal to the estuarine response time, but the event in 1996 was much shorter and lasted only 1/4 the estuarine response time. For snow melt freshets with broad discharge peaks, the high-discharge period greatly exceeds the estuarine response time. For winter rain and late summer hurricanes (e.g., hurricanes in 1927, 1938, and 1955), the runoff period is often too brief for the estuary to adjust and sediment export is less than would occur in a freshet with similar Q_r .

Estuarine Turbidity Maxima

The results show both along-channel and across-channel gradients in sediment resuspension and transport. Estuarine circulation in the channel produces a local maximum in up-estuary transport in the channel of the lower ETM (Figs. 7 and 15). The convergence of along-estuary sediment flux could provide a supply of sediment for tidal resuspension to maintain the high concentrations of suspended sediment observed there (Geyer et al. 2001; Traykovski et al. 2004). During low-discharge periods in the summer, the region of up-estuary transport in the channel expands northward to upper Haverstraw Bay (55–60 km) where an upper estuary ETM has also been observed (Bokuniewicz and Arnold 1984; Figs. 7 and 15). The formation of the upper ETM may be seasonal with the northward extension of the salinity field during low flow conditions. The location of an ETM depends not only on a convergence of sediment flux, but also on a supply of bed material for resuspension (Sanford et al. 2001). Consequently, the formation of the upper ETM may lag the expansion of the salinity field by several spring–neap cycles as the mean currents redistribute the supply of erodible material.

Fig. 15 Sediment flux in the lower estuary (16 km), including fluvial supply (black), estuarine transport (gray), and the sum for the net transport (gray squares, bin averaged). Lines show best fits to the fluvial (cubic polynomial) and estuarine (linear) components, and the sum of the two for the net transport



Model Uncertainty

Model assumptions and uncertainties can substantially influence these results, and additional model validation is needed. Foremost, the results are sensitive to the erosion parameters, yet we lack sufficient spatial or temporal observations of bed erodibility to define the erosion parameters *a priori*. The long-term equilibrium constraint permits an estimate of the lateral variability in erodibility that appears to be consistent with observations, but the approach simplifies a system with heterogeneous bed composition ranging from unconsolidated mud to sand, gravel, or shell fragments (Woodruff et al. 2001; Klingbeil and Sommerfield 2005; Nitsche et al. 2007).

To limit the degrees of freedom, we held U_c constant and searched for C_0 that satisfied the equilibrium transport constraint, but the solution is not unique. We started with an initial C_0 based on observations at a point (Traykovski et al. 2004), and then searched for C_0 that both allowed equilibrium transport and minimized the difference between the final and the initial C_0 . Other approaches are plausible,

such as beginning with along-estuary variability in C_0 or allowing U_c and C_0 to co-vary. Similarly, we incorporated a seasonal scaling factor to represent the increased erodibility of sediment from winter storm events. An alternative formulation might be to quantify and track a mobile pool of sediment trapped after discharge events, including coupling to the time dependence of erodibility. In general, the bed erosion parameters remain underconstrained and these results may not be unique or locally optimal. However, the larger scale and longer period patterns of sediment transport that are our focus are less sensitive to these uncertainties than are the local near-bottom suspended sediment concentration.

In addition to erodibility, the sediment fluxes depend on the suspended load at the estuarine boundaries. The rating curves for fluvial sediment load provide a better estimate than single year of observations, but the observations used to derive the curves span an order of magnitude for a given Q_r (Woodruff 1999). The long-term supply of marine sediment from New York Harbor is poorly documented, and it is likely to vary seasonally with discharge (Hirschberg

et al. 1996; Feng et al. 1999; Woodruff et al. 2001). Storage of sediment in the Harbor and subsequent flux back into the lower estuary may increase the overall residence time in the system.

By distinguishing between channel and shoals, the model incorporates lateral depth variability that affects the along-estuary sediment fluxes. However, the model does not account for lateral circulation that redistributes momentum and stratification at tidal timescales and may contribute to sediment trapping in the lower ETM (Geyer et al. 1998; Traykovski et al. 2004). Lateral estuarine dynamics remain poorly understood, so incorporating lateral flows into the tidally averaged model with low spatial resolution remains a challenge. Similarly, the sediment flux calculations are sensitive to the vertical structure of the suspended sediment. We have formulated the sediment profile as a function of settling velocity that can vary over orders of magnitude in space and time, but alternative formulations are also plausible. Additional observations and robust formulations for suspended sediment profiles would improve the predictive ability of the model.

Simulations would be enhanced by linking the sediment transport explicitly with estuarine morphology. Modifications due to dredging or bank erosion can provide a significant sink or source of sediment independent of sea level rise or fluvial input (Klingbeil and Sommerfield 2005). Historical changes in bathymetry may modify estuarine and river velocities, and thus the regions of expected trapping and deposition. Effects of major shifts in bathymetry such as a cessation of dredging and subsequent infilling could potentially be addressed with this model, but to completely represent the feedbacks among morphology, sediment transport, and hydrodynamics would require resolution at tidal timescales.

Despite the limitations, the model results are supported by correspondence with observations of sediment flux (Geyer et al. 1998; Traykovski et al. 2004) and bottom properties (Nitsche et al. 2007). The simple model framework permits simulations over extended periods to quantify long-term patterns and capture episodic events. Once identified by the simple model, the episodic transport events should be examined in greater detail using 3D hydrodynamic and sediment transport models. Note that both the simple model and a 3D hydrodynamic simulation remain limited by the lack of data to parameterize bed properties, boundary sediment fluxes, and salinity at the open boundary (Warner et al. 2005).

Summary

Infrequent, extreme discharge events are critical to the long-term sediment budget in estuaries. Elevated river discharge

enhances down-estuary sediment transport through the mean velocity, but the transport capacity depends on the timing and duration of discharge events. Discharge events during spring tides have greater down-estuary transport because of reduced estuarine circulation and sediment trapping. Spring freshets when the period of elevated discharge exceeds the estuarine response time have proportionally greater down-estuary transport than isolated storms.

Extreme discharge events also supply large amounts of sediment to the estuary, and the sediment load has a nearly cubic dependence on discharge. Sediment transport capacity in the estuary is nearly linear with discharge, so the discrepancy between sediment supply and export leads to periods of sediment excess or deficit in the estuary. On average, the estuary accumulates sediment during low- and high-discharge periods and exports sediment during moderate discharge periods. The intermittency of droughts and wet periods determines sediment residence time in the estuary.

Lateral gradients in water depth produce lateral gradients in estuarine sediment transport capacity, with greater up-estuary transport in the deeper channel due to enhanced baroclinic circulation. On the shoals sediment transport is predominantly down-estuary, but lateral gradients in sediment erodibility are required for the net transport to balance the sediment input from the river. Model calculations based on an assumption of long-term equilibrium transport indicate that bed erodibility on the shoals must be significantly greater than in the channel. The model results are consistent with observations of sediment flux and bed properties.

Acknowledgments This research was supported by the Hudson River Foundation through grant #005/05A.

Appendix

Near-bottom velocities are less than the surface magnitudes from tidal harmonics, so we use coefficients to calculate near-bottom, tidal maximum velocities:

$$U_{\text{flood}} = f_1(U_t - U_0) + f_2 U_e \quad (\text{A1})$$

$$U_{\text{ebb}} = f_1(U_t + U_0) - f_2 U_e$$

where f_1 modifies the parabolic velocity magnitudes and f_2 modifies the cubic velocity. We fit the coefficients based on velocity data from the Hudson, comparing model results with observations. The velocity profiles depend on fractional depth ($z/H = \{0, -1\}$), so we define “near-bottom” as a distance above the bed equal to 20% of the water depth ($z/H = -0.8$).

To calculate f_1 , we add Eq. A1 such that $\frac{1}{2}(U_{\text{flood}} + U_{\text{ebb}}) = f_1 U_t$. Plotting the sum of observed flood and ebb

Fig. 16 **a** Schematic description of ebb ($f_1(U_t+U_0)-f_2U_e$) and flood ($f_1(U_t-U_0)-f_2U_f$) velocity profiles based on polynomial shape functions. **b** Near-bottom velocities at four stations during 2004, plotting $1/2(U_{\text{ebb}}+U_{\text{flood}})_O$ against $U_{t|M}$, where “O” indicates observations and “M” indicates model results; the slope is the factor modifying parabolic velocity profile, f_1 . **c** Near-bottom velocities at four stations during 2004, plotting $1/2[2f_1U_{0|M}-(U_{\text{ebb}}-U_{\text{flood}})_O]$ against $U_{t|M}$; slope is factor modifying cubic velocity profile, f_2 . f_2 is different for each station depending on cross-section shape, as shown in Fig. 17

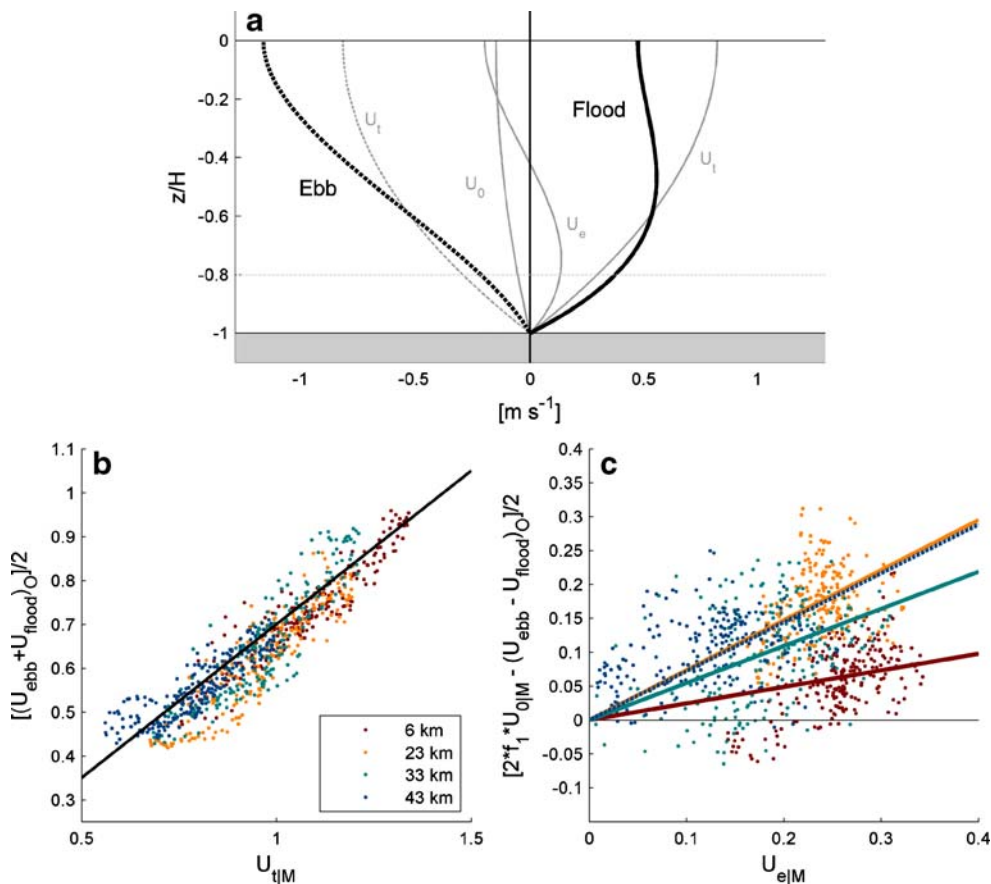
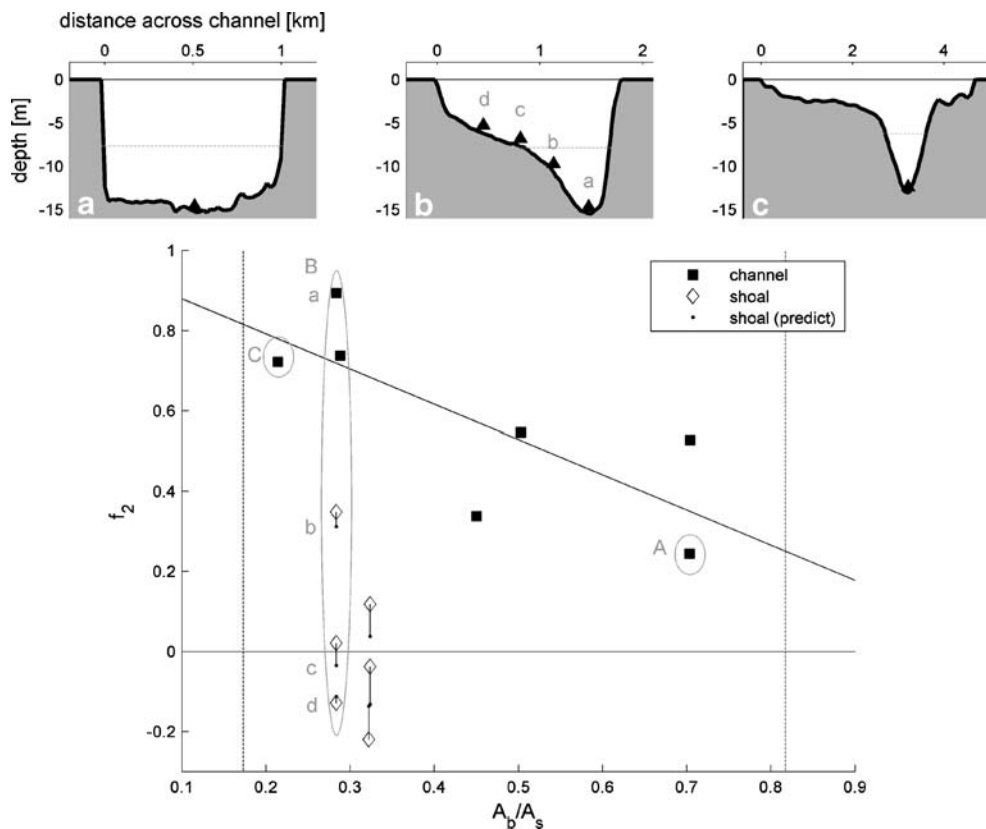


Fig. 17 Estuarine velocity factor (f_2) as a function of cross-section shape. A_b is near-bottom area (flow area below $H/2$) and A_s is near-surface area (above $H/2$). The values of f_2 are from linear regressions at locations along the Hudson as shown in Fig. 16. Solid squares are observations in the thalweg, while open diamonds are from stations on shoals. Dots connected by lines are predicted f_2 on the shoals based on A_b/A_s and the depth relative to the thalweg. Top three panels show cross-sections spanning a range of A_b/A_s . Reference line is the best fit used to define f_2 based on A_b/A_s (Eq. A2) to calculate near-bottom velocities in the model (Eq. A1). Vertical dashed lines indicate range of A_b/A_s in the Hudson



near-bottom velocities against U_t we find the slope f_1 . In the observations f_1 was about 0.7, to within about 10% (Fig. 16). To account for lateral shear in the tidal velocity, we assume the cross-channel structure of tidal velocity is proportional to the square root of the local depth: $U_t(y) = \langle U_t \rangle \frac{h^{1/2}(h)}{\langle h^{3/2} \rangle}$, where h is the local depth and brackets represent cross-section averages (Smith 1983).

We estimate f_2 by subtracting Eq. A1 so that $\frac{1}{2}((U_{\text{flood}} - U_{\text{ebb}}) + 2f_1 U_0) = f_2 U_e$. Again, the slope of $\frac{1}{2}((U_{\text{flood}} - U_{\text{ebb}}) + 2f_1 U_0)$ versus U_e (using observed U_{flood} and U_{ebb} and modeled U_0 and U_e) is fit to find f_2 . We find that f_2 varies spatially depending both on cross-sectional shape and the local water depth relative to the thalweg. Cross-sections that have a narrow, deep channel and broad, shallow shoals have higher f_2 values in the thalweg than cross-sections with relatively uniform depth. We quantify this by plotting f_2 as a function of the ratio of near-bottom cross-sectional area (flow area below $H/2$, where H is the thalweg depth) to near-surface cross-sectional area (flow area above $H/2$; Fig. 17). The ratio A_b/A_s has a maximum of 1 for a rectangular channel, but in the Hudson the ratio ranges between 0.82 (for a laterally uniform region near the Battery) and 0.17 (for a narrow, deep channel with broad shoals, as in the Tappan Zee). The f_2 for calculating near-bottom velocities is based on a linear fit of the observed f_2 (found from regression fits as in Fig. 16c) to the ratio A_b/A_s :

$$f_2 = -0.89 A_b/A_s + 0.97, \quad (\text{A2})$$

yielding a range of f_2 from 0.24 to 0.82. Conceptually, the up-estuary volume flux due to estuarine circulation ($\sim U_e A_b$) should balance the down-estuary volume flux ($U_e A_s$). The magnitude of U_e depends on the thalweg depth, so in cross-sections with narrow, deep channels (small A_b/A_s), measured velocities near the bed will be greater than in laterally uniform channels with equivalent U_e . To project the estuarine velocity profile onto the shoals, we use the velocity in the thalweg (including the direction of flow) that corresponds with the near-bottom depth on the shoals. We compared f_2 on the shoals predicted from the lateral projection of Eq. A2 against f_2 from regression fits of observations (as in Fig. 16c) and found good agreement in the six available cases (Fig. 17).

References

- Abood, K.A. 1974. Circulation in the Hudson Estuary. *Annals of the New York Academy of Sciences* 250(1): 39–111. doi:10.1111/j.1749-6632.1974.tb43895.x.
- Bokuniewicz, H.J. and C.L. Arnold. 1984. Characteristics of suspended sediment transport in the lower Hudson River. *Northeastern Environmental Science* 3(3/4): 184–189.
- Bokuniewicz, H.J. and J.M. Ellsworth. 1986. Sediment budget for the Hudson system. *Northeastern Geology* 8(3): 156–164.
- Bowen, M.M. and W.R. Geyer. 2003. Salt transport and the time-dependent salt balance of a partially stratified estuary. *Journal of Geophysical Research* 108(C5): 3158.
- Carbotte, S.M., R.E. Bell, W.B.F. Ryan, C. McHugh, A. Slagle, F. Nitsche, and J. Rubenstein. 2004. Environmental change and oyster colonization within the Hudson River estuary linked to Holocene climate. *Geo-Marine Letters* 24(4): 212–224. doi:10.1007/s00367-004-0179-9.
- Cook, T.L., C.K. Sommerfield, and K. Wong. 2007. Observations of tidal and springtime sediment transport in the upper Delaware Estuary. *Estuarine, Coastal and Shelf Science* 72(1–2): 235–246. doi:10.1016/j.ecss.2006.10.014.
- Ellsworth, J.M. 1986. Sources and sinks for fine-grained sediment in the lower Hudson River. *Northeastern Geology* 8(3): 141–155.
- Feng, H., J.K. Cochran, D.J. Hirschberg, and R.E. Wilson. 1998. Small-scale spatial variations of natural radionuclide and trace metal distributions in sediments from the Hudson River Estuary. *Estuaries* 21(2): 263–280.
- Feng, H., J.K. Cochran, and D.J. Hirschberg. 1999. 234Th and 7Be as tracers for the transport and dynamics of suspended particles in a partially mixed estuary. *Geochimica et Cosmochimica Acta* 63 (17): 2487–2505. doi:10.1016/S0016-7037(99)00060-5.
- Foreman, M. 1978. *Manual for tidal currents analysis and prediction*. Patricia Bay: Institute of Ocean Sciences.
- Geyer, W.R., R.P. Signell, and G.C. Kineke. 1998. Lateral trapping of sediment in partially mixed estuary. In *Physics of estuaries and coastal seas: proceedings of the 8th International Biennial Conference on physics of estuaries and coastal seas*, 115–124.
- Geyer, W.R., J.D. Woodruff, and P. Traykovski. 2001. Sediment transport and trapping in the Hudson River Estuary. *Estuaries* 24 (5): 670–679.
- Hansen, D.V. and M. Rattray. 1965. Gravitational circulation in straits and estuaries. *Journal of Marine Research* 23: 104–122.
- Hetland, R.D. and W.R. Geyer. 2004. An idealized study of the structure of long, partially mixed estuaries. *Journal of Physical Oceanography* 34(12): 2677–2691.
- Hirschberg, D.J., P. Chin, H. Feng, and J.K. Cochran. 1996. Dynamics of sediment and contaminant transport in the Hudson River Estuary: Evidence from sediment distributions of naturally occurring radionuclides. *Estuaries* 19(4): 931–949.
- Kirkby, M. and N. Cox. 1995. A climatic index for soil erosion potential (CSEP) including seasonal and vegetation factors. *CATENA* 25(1–4): 333–352. doi:10.1016/0341-8162(95)00016-L.
- Klingbeil, A.D. and C.K. Sommerfield. 2005. Latest Holocene evolution and human disturbance of a channel segment in the Hudson River Estuary. *Marine Geology* 218(1–4): 135–153. doi:10.1016/j.margeo.2005.02.026.
- Kranenburg, C. 1986. A time scale for long-term salt intrusion in well-mixed estuaries. *Journal of Physical Oceanography* 16(7): 1329–1331.
- Lerczak, J.A., W.R. Geyer, and R.J. Chant. 2006. Mechanisms driving the time-dependent salt flux in a partially stratified estuary. *Journal of Physical Oceanography* 36(12): 2296–2311.
- MacCready, P. 2004. Toward a unified theory of tidally-averaged estuarine salinity structure. *Estuaries and Coasts* 27(4): 561–570. doi:10.1007/BF02907644.
- MacCready, P. 2007. Estuarine adjustment. *Journal of Physical Oceanography* 37(8): 2133–2145.
- McHugh, C.M., S.F. Pekar, N. Christie-Blick, W.B. Ryan, S. Carbotte, and R. Bell. 2004. Spatial variations in a condensed interval between estuarine and open-marine settings: Holocene Hudson River estuary and adjacent continental shelf. *Geology* 32(2): 169–172. doi:10.1130/G20150.1.

- Meade, R.H. 1969. Landward transport of bottom sediments in estuaries of the Atlantic Coastal Plain. *Journal of Sedimentary Petrology* 39(1): 222–234.
- Monismith, S.G., W. Kimmerer, J.R. Burau, and M.T. Stacey. 2002. Structure and flow-induced variability of the subtidal salinity field in Northern San Francisco Bay. *Journal of Physical Oceanography* 32(11): 3003–3019.
- Nash, D.B. 1994. Effective sediment-transporting discharge from magnitude-frequency analysis. *Journal of Geology* 102(1): 79–96.
- Nitsche, F.O., R. Bell, S.M. Carbotte, W.B.F. Ryan, and R. Flood. 2004. Process-related classification of acoustic data from the Hudson River Estuary. *Marine Geology* 209(1–4): 131–145. doi:[10.1016/j.margeo.2004.05.023](https://doi.org/10.1016/j.margeo.2004.05.023).
- Nitsche, F., W. Ryan, S. Carbotte, R. Bell, A. Slagle, C. Bertinado, R. Flood, T. Kenna, and C. McHugh. 2007. Regional patterns and local variations of sediment distribution in the Hudson River Estuary. *Estuarine, Coastal and Shelf Science* 71(1–2): 259–277. doi:[10.1016/j.ecss.2006.07.021](https://doi.org/10.1016/j.ecss.2006.07.021).
- Olsen, C.R. 1979. Radionuclides, sedimentation and the accumulation of pollutants in the Hudson River Estuary. Ph.D., Columbia University.
- Olsen, C.R., H.J. Simpson, R.F. Bopp, S.C. Williams, T.H. Peng, and B.L. Deck. 1978. A geochemical analysis of the sediments and sedimentation in the Hudson Estuary. *Journal of Sedimentary Research* 48(2): 401–418.
- Olsen, C.R., I.L. Larsen, P.J. Mulholland, K.L. Von Damm, J.M. Grebmeier, L.C. Schaffner, R.J. Diaz, and M.M. Nichols. 1993. The concept of an equilibrium surface applied to particle sources and contaminant distributions in estuarine sediments. *Estuaries* 16(3): 683–696.
- Panuzio, F.L. 1965. Lower Hudson River siltation. In *Proceedings of the 2nd Federal Interagency Sedimentation Conference*, 512–550. Agricultural Research Service Misc. Publication 970.
- Partheniades, E. 1965. Erosion and deposition of cohesive soils. *Journal of the Hydraulics Division, American Society of Civil Engineers* 91(HY2): 105–138.
- Pawlowicz, R., B. Beardsley, and S. Lentz. 2002. Classical tidal harmonic analysis including error estimates in MATLAB using T_TIDE. *Computers & Geosciences* 28(8): 929–937. doi:[10.1016/S0098-3004\(02\)00013-4](https://doi.org/10.1016/S0098-3004(02)00013-4).
- Postma, H. 1967. Sediment transport and sedimentation in the estuarine environment. In *Estuaries*, 158–179. Washington, DC: American Association for the Advancement of Science.
- Ralston, D.K., W.R. Geyer, and J.A. Lerczak. 2008. Subtidal salinity and velocity in the Hudson River Estuary: Observations and modeling. *Journal of Physical Oceanography* 38(4): 753–770.
- Sanford, L., S. Suttles, and J. Halka. 2001. Reconsidering the physics of the Chesapeake Bay estuarine turbidity maximum. *Estuaries and Coasts* 24(5): 655–669. doi:[10.1007/BF02804824](https://doi.org/10.1007/BF02804824).
- Schubel, J.R., and D.J. Hirschberg. 1978. Estuarine graveyards, climatic change, and the importance of the estuarine environment. In *Estuarine Interactions*, 285–303. New York: Academic Press.
- Schureman, P. 1959. *Manual of harmonic analysis and prediction of tides*. Washington, DC: U.S. Department of Commerce, Coast and Geodetic Survey.
- Slagle, A., W. Ryan, S. Carbotte, R. Bell, F. Nitsche, and T. Kenna. 2006. Late-stage estuary infilling controlled by limited accommodation space in the Hudson River. *Marine Geology* 232(3–4): 181–202. doi:[10.1016/j.margeo.2006.07.009](https://doi.org/10.1016/j.margeo.2006.07.009).
- Smith, R. 1983. Longitudinal dispersion coefficients for varying channels. *Journal of Fluid Mechanics* 130: 299–314.
- Sommerfield, C.K. 2006. On sediment accumulation rates and stratigraphic completeness: Lessons from Holocene ocean margins. *Continental Shelf Research* 26(17–18): 2225–2240. doi:[10.1016/j.csr.2006.07.015](https://doi.org/10.1016/j.csr.2006.07.015).
- Stedfast, D.A. 1980. *Cross sections of the Hudson River Estuary from Troy to New York City*. New York: USGS.
- Traykovski, P., R. Geyer, and C. Sommerfield. 2004. Rapid sediment deposition and fine-scale strata formation in the Hudson estuary. *Journal of Geophysical Research* 109: F02004. doi:[10.1029/2003JF000096](https://doi.org/10.1029/2003JF000096).
- Wall, G., E. Nystrom, and S. Litten. 2008. Suspended sediment transport in the freshwater reach of the Hudson River Estuary in Eastern New York. *Estuaries and Coasts*. doi:[10.1007/s12237-008-9050-y](https://doi.org/10.1007/s12237-008-9050-y). <http://dx.doi.org/10.1007/s12237-008-9050-y>.
- Warner, J.C., W.R. Geyer, and J.A. Lerczak. 2005. Numerical modeling of an estuary: A comprehensive skill assessment. *Journal of Geophysical Research* 110: C05001. doi:[10.1029/2004JC002691](https://doi.org/10.1029/2004JC002691).
- Woodruff, J.D. 1999. Sediment deposition in the lower Hudson River estuary. M.S. thesis, Massachusetts Institute of Technology/Woods Hole Oceanographic Institution.
- Woodruff, J.D., W.R. Geyer, C.K. Sommerfield, and N.W. Driscoll. 2001. Seasonal variation of sediment deposition in the Hudson River estuary. *Marine Geology* 179(1–2): 105–119. doi:[10.1016/S0025-3227\(01\)00182-7](https://doi.org/10.1016/S0025-3227(01)00182-7).